

Large Language Models are Powerful Electronic Health Record Encoders

Stefan Hegselmann^{1,2†}, Georg von Arnim^{1†}, Tillmann Rheude¹,
Noel Kronenberg¹, David Sontag^{3,4}, Gerhard Hindricks²,
Roland Eils^{1,5}, Benjamin Wild¹

¹Berlin Institute of Health at Charité – Universitätsmedizin Berlin,
Center of Digital Health, Berlin, Germany.

²Deutsches Herzzentrum der Charité – Medical Heart Center of Charité
and German Heart Institute Berlin, Berlin, Germany.

³Computer Science and Artificial Intelligence Laboratory (CSAIL),
Massachusetts Institute of Technology (MIT), Cambridge, MA, USA.

⁴Layer Health, Inc., MA, USA.

⁵Intelligent Medicine Institute, Fudan University, Shanghai, China.

†These authors contributed equally to this work.

Abstract

Electronic Health Records (EHRs) offer considerable potential for clinical prediction, but their complexity and heterogeneity present significant challenges for traditional machine learning methods. Recently, domain-specific EHR foundation models trained on large volumes of unlabeled EHR data have shown improved predictive accuracy and generalization. However, their development is constrained by limited access to diverse, high-quality datasets, and inconsistencies in coding standards and clinical practices. In this study, we explore the use of general-purpose Large Language Models (LLMs) to encode EHR into high-dimensional representations for downstream clinical prediction tasks. We convert structured EHR data into Markdown-formatted plain-text documents by replacing medical codes with natural language descriptions. This enables the use of LLMs and their extensive semantic understanding and generalization capabilities as effective encoders of EHRs without requiring access to private medical training data. We show that LLM-based embeddings can often match or even surpass the performance of a specialized EHR foundation model, CLMBR-T-Base, across 15 diverse clinical tasks from the EHRSHOT benchmark. Critically, our approach requires no institution-specific training and can incorporate any medical code with a text description, whereas existing EHR foundation models

operate on fixed vocabularies and can only process codes seen during pretraining. To demonstrate generalizability, we further evaluate the approach on the UK Biobank (UKB) cohort, out-of-domain for CLMBR-T-Base, whose fixed vocabulary covers only 16% of UKB codes. Notably, an LLM-based model achieves superior performance for prediction of disease onset, hospitalization, and mortality, indicating robustness to population and coding shifts. Our findings suggest that repurposed general-purpose LLMs for EHR encoding provide a scalable and flexible alternative to domain-specific models for clinical prediction.

Keywords: electronic health records, clinical prediction, machine learning, large language models, foundation models

1 Introduction

EHRs are now widely used in modern healthcare, providing comprehensive, longitudinal views of a patient’s health status [1]. Machine learning methods can use this rich data for risk stratification and to support clinical decision-making [2–4]. In recent years, researchers have explored a variety of prediction tasks based on EHRs, including hospital readmission [5, 6], length of hospital stay [6], sepsis onset detection [7, 8], mortality prediction [6, 9], discharge diagnoses [6], and heart failure outcomes [10]. The overarching goal is to harness EHR data using machine learning to improve clinical outcomes and reduce healthcare costs.

However, machine learning on EHR data poses significant challenges due to its inherent complexity. EHR data is characterized by variable-length sequences of patient visits, irregular sampling intervals, missing entries, heterogeneous and noisy information, and a wide range of hierarchical medical concepts [11]. As a result, deep learning models often achieve only modest improvements over traditional methods such as logistic regression or tree-based models for EHR prediction tasks [6, 12, 13]. To mitigate these issues, recent approaches have employed large-scale foundation models that are pretrained on unlabeled EHR data using unsupervised learning [14]. Many of these models adopt strategies from natural language processing, such as masked word prediction as in BERT [15] or autoregressive next word prediction as in GPT [16]. Treating EHR data as sequences of medical codes enables analogous methods such as masked code prediction [12, 17–19] or next code prediction [13, 20, 21]. However, code-based EHR foundation models face two fundamental obstacles to interoperability and generalization: site-specific coding practices and fixed vocabularies learned during pretraining. For example, CLMBR-T-Base [13] supports only 26,249 unique codes from its training corpus, and when applied to the UKB with 50,702 unique medical codes, only 7,969 (16%) could be mapped, leaving 84% of codes unseen by the model. Achieving interoperability would require pretraining on diverse EHR datasets from many institutions, which is difficult due to the sensitivity of healthcare data. This motivates models that operate on natural-language descriptions of clinical codes, which avoid fixed vocabularies and transfer more readily across institutions.

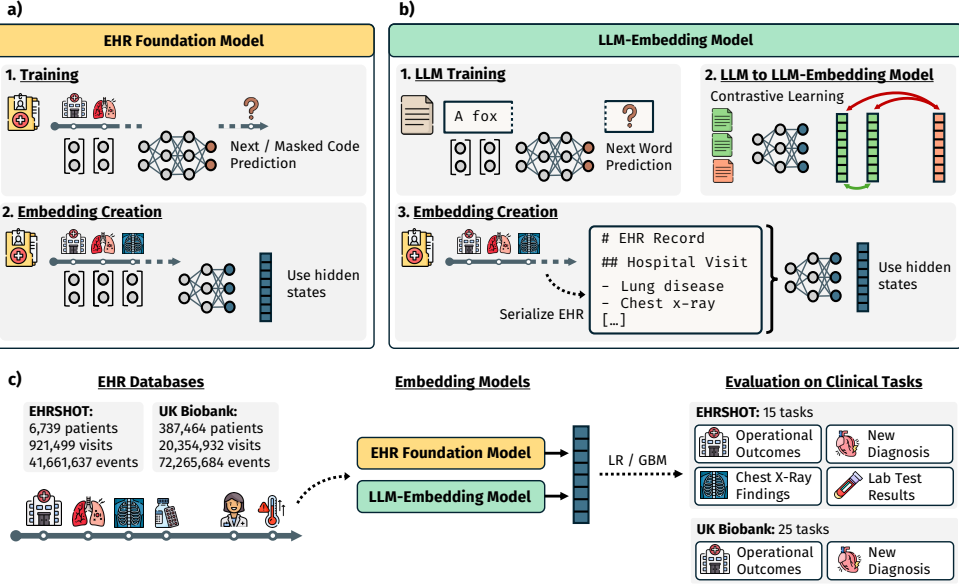


Fig. 1 Study Overview. (a) EHR foundation models are pretrained on unlabeled EHR data. Common unsupervised learning tasks are masked code or next code prediction. To obtain a representation for an EHR, we use the hidden states of the pretrained model. (b) LLMs are pretrained on vast amounts of text data. To obtain an LLM embedding model, architectural changes are applied, and contrastive learning is used to improve representational performance. To obtain an EHR embedding, the data is first serialized as text and then processed by the LLM embedding model. Again, we use the hidden states for the embedding. (c) We use the EHRSHOT benchmark and the UK Biobank (UKB) cohort for our experiments. Medical events of each patient are converted into numerical embeddings using an EHR foundation model and an LLM embedding model, respectively. A logistic regression (LR) model is trained, validated, and tested for each clinical prediction task. We also test a Gradient Boosted Machine (GBM) prediction model for the count-based baseline. Icons from flaticon.com.

LLMs benefit from pretraining on vast general-purpose text corpora and a broad range of natural-language tasks [22, 23]. This extensive pretraining enables their language comprehension and allows them to capture domain-agnostic patterns that can be adapted for healthcare applications. Consequently, LLMs have demonstrated strong performance in extracting medical concepts [24], summarizing medical texts [25], and predicting medical outcomes [26], even in low-resource settings. Recent work extends LLMs to structured EHR by serializing records into text and either using model generations for prediction [27–32] or extracting fixed-dimensional embeddings for downstream classifiers [33–35]. While both paradigms can be competitive with common baselines, many prior studies only use short context windows and evaluate on private or emergency-department cohorts, limiting longitudinal coverage and external validity [33–35] (see Section 4.7). Moreover, most modern LLMs, such as GPT [36] and Qwen [37, 38], use decoder-only transformer architectures trained with left-to-right objectives, which are not optimized for representation learning. To address this limitation, recent work converts decoder-only LLMs into effective LLM embedding models

Table 1 Cohort Overview. Summary statistics for EHRSHOT and UK Biobank, including the number of patients, visits, events, and patient characteristics.

Attribute	EHRSHOT	UK Biobank
Num Patients	6,739	387,464
Num Visits	921,499	19,484,777
Num Events	41,661,637	72,265,684
Num Female	3,441	214,565
Num Male	3,298	172,899
Age, mean \pm SD	59.3 \pm 17.9	56.78 \pm 8.11
American Indian	25	0
Asian	1,043	8,659
Black	298	5,751
Pacific Islander	74	0
Unknown	1,563	7,202
White	3,736	365,888
Hispanic	1,038	-
Non-Hispanic	5,701	-

via contrastive learning or related techniques [39–43]. Additionally, these state-of-the-art models offer large context windows, making them well-suited for handling long inputs such as serialized EHR data.

In this study, we evaluate whether general-purpose LLM embedding models can effectively encode EHR data for clinical prediction [44] (see Fig. 1). To this end, we convert structured EHR records into plain-text summaries that highlight key patient information at prediction time. Using a state-of-the-art LLM embedding model, Qwen3-Embedding-8B (Qwen3-Emb-8B) [38, 43] with a context size of 8,192 tokens, we generate high-dimensional EHR embeddings that serve as inputs to logistic regression classifiers across 15 clinical tasks from the EHRSHOT benchmark. We analyze the performance in the few-shot setting, where the downstream logistic regression is trained with only a small number of labeled examples, to evaluate the generalization of this approach, and we conduct extensive ablation studies to identify the components that drive the LLM’s effectiveness. Finally, we validate our approach on the UKB for predicting mortality, hospitalization, and the onset of 23 diseases [45] to assess robustness and compare its generalizability against EHR-specific foundation models.

2 Results

2.1 Experimental Setup

Our primary analysis was conducted using the EHRSHOT benchmark, which contains EHRs from 6,739 adult patients treated at Stanford Health Care and Lucile Packard Children’s Hospital between 1990 and 2023. This dataset includes 921,499 visits and over 41.6 million clinical events [44], and serves as a standardized benchmark with 15 clinical prediction tasks organized into 4 task groups, along with predefined splits and publicly available code. Table 1 summarizes cohort statistics, and task details are shown in Table 2. Further information on task definitions and preprocessing is provided in Section 4.1.

For external validation, we used the UKB, a population-based cohort comprising 502,489 UK participants [46, 47]. This allowed us to evaluate the generalizability of

Table 2 EHRSHOT Prediction Tasks Overview. The EHRSHOT benchmark defines 15 clinical prediction tasks spanning four different task groups. The number of examples per task differs based on the prevalence and frequency of clinical events. Canonical splits for training, validation, and testing are defined to ensure reproducible experiments [44].

Attribute	Train Labels (Positive)	Valid Labels (Positive)	Test Labels (Positive)	Total Labels (Positive)
Operational Outcomes				
Long Length of Stay	2,569 (681)	2,231 (534)	2,195 (552)	6,995 (1,767)
30-day Readmission	2,609 (370)	2,207 (281)	2,189 (260)	7,005 (911)
ICU Transfer	2,402 (113)	2,052 (92)	2,037 (85)	6,491 (290)
Anticipating Lab Test Results				
Thrombocytopenia	68,776 (9,774)	54,504 (6,962)	56,338 (7,960)	179,618 (24,696)
Hyperkalemia	76,349 (1,215)	60,168 (886)	63,653 (948)	200,170 (3,049)
Hypoglycemia	122,108 (1,065)	95,488 (858)	100,568 (783)	318,164 (2,706)
Hyponatremia	81,336 (20,181)	64,473 (14,674)	67,028 (16,003)	212,837 (50,858)
Anemia	70,501 (9,544)	56,224 (7,445)	58,155 (7,636)	184,880 (24,625)
Assignment of New Diagnoses				
Hypertension	1,260 (184)	1,250 (177)	1,261 (160)	3,771 (521)
Hyperlipidemia	1,684 (205)	1,441 (189)	1,317 (172)	4,442 (566)
Pancreatic Cancer	2,576 (155)	2,215 (53)	2,220 (56)	7,011 (264)
Celiac	2,623 (62)	2,284 (11)	2,222 (21)	7,129 (94)
Lupus	2,570 (104)	2,226 (33)	2,243 (20)	7,039 (157)
Acute MI	2,534 (175)	2,177 (146)	2,127 (144)	6,838 (465)
Anticipating Chest X-ray Findings				
Chest X-Ray Findings	7,481 (4,771)	9,366 (6,032)	9,428 (6,400)	26,275 (17,203)

our approach across healthcare systems, especially since the CLMBR-T-Base model was trained on data from the same hospital system as EHRSHOT. Due to structural differences between the datasets, not all EHRSHOT tasks were transferable to the UKB (see Section 4.10). We thus focused on predicting one-year risk of hospitalization, mortality, and the onset of 23 diseases [45] for the external validation in the UKB. The processed UKB subset used in our study consisted of 387,464 patients, approximately 19.5 million visits, and over 72 million clinical events. Table 7 provides task descriptions and label distributions.

To prepare EHR data for use with LLMs, we serialized structured patient records into plain text formatted in Markdown, with a maximum length of 8,192 tokens, prioritizing more recent data. For EHRSHOT, serialization began with a reference prediction date to which all event dates were normalized, followed by demographics, recent values for 24 key Logical Observation Identifiers Names and Codes (LOINC) concepts across Body Metrics, Vital Signs, and Lab Results, including units and classification (low/normal/high). These were followed by a summary of patient visits and reverse-chronological listings of visit-level events such as conditions, medications, and procedures. An example EHR text serialization is shown in Fig. 2, and a detailed explanation appears in Section 4.2. For UKB, a similar serialization approach was used, with event dates normalized to each patient’s recruitment date and exclusion of detailed measurements due to data limitations. In some experiments, we used a 4,096-token limit to accommodate runtime constraints.

```

# Electronic Healthcare Record
Current time: [2024-01-01](2024-01-01)

## Patient Demographics
- Patient age: 78
- Black
- FEMALE
- Hispanic or Latino

## Recent Body Metrics
- Body weight (oz): 1801
- Body height (inch): 62.0, 61.0
- Body mass index / BMI (kg/m2): 18.7 (normal)
- Body surface area (m2): 1.47

## Recent Vital Signs
- Heart rate (bpm): 121 (high), 85 (normal)
- Respiratory rate (breaths/min): 16 (normal)
- Systolic blood pressure (mmHg): 148 (high), 117 (normal)
- Diastolic blood pressure (mmHg): 81 (normal), 57 (low)
- Body temperature (°F): 97.4 (normal), 98.8 (normal)
- Oxygen saturation (%): 97 (normal), 97 (normal), 99 (normal)

## Recent Lab Results
- Hemoglobin (g/dL): 8.2 (low), 8.6 (low), 8.8 (low)
- Hematocrit (%): 24 (low), 26 (low), 26 (low)
- Erythrocytes: No recent data
- Leukocytes (10^3/uL): 2.7 (low), 8.8 (normal), 6.2 (normal)
- Platelets (10^3/uL): 215 (normal), 199 (normal)
- Sodium (mmol/L): 132 (low)
- Potassium (mmol/L): 4.2 (normal), 4.4 (normal)
- Chloride (mmol/L): 95 (low), 102 (normal)
- Carbon dioxide, total (mmol/L): No recent data
- Calcium (mg/dL): 8.9 (low), 8.5 (low)
- Glucose (mg/dL): 92 (normal), 112 (high)
- Urea nitrogen (mg/dL): 11 (normal), 8 (normal)
- Creatinine (mg/dL): 0.4 (low), 0.7 (normal)
- Anion gap: No recent data

## Past Medical Visits
- Inpatient Visit on [2023-12-17](2023-12-17) (14 days before prediction time, current visit)
- Office Visit on [2023-10-27](2023-10-27) (65 days before prediction time)

## General Medical Events
- Cigarette consumption: N, N, N
- Mitral valve disorder

## Detailed Past Medical Visits (most recent first)
### Inpatient Visit on [2023-12-17](2023-12-17) (14 days before prediction time, current visit)
#### Conditions
- Acute posthemorrhagic anemia
- Partial thromboplastin time, activated
- pH measurement, venous: 7.25, 7.31, 7.31

#### Medications
- furosemide 20 MG Oral Tablet
- pantoprazole 20 MG Delayed Release Oral Tablet

#### Procedures
- Chest x-ray
- Electrocardiogram report

### Office Visit on [2023-10-27](2023-10-27) (65 days before prediction time)
[...]

```

Fig. 2 Example EHR Text Serialization. The EHR data is serialized into plain text to apply LLM embedding models. We use Markdown formatting and prioritize relevant medical information. All dates were normalized relative to a reference date. Next, the patient's demographics are listed. Time-series data coded via Logical Observation Identifiers Names and Codes (LOINC) was aggregated into 24 key concepts listed with the last three values, units, and classifications into low, normal, and high. Then, a list of all visits and all concepts not associated with a visit are given. Lastly, detailed visit entries beginning with the most recent are listed. Unique concepts are categorized into conditions, medications, and procedures. The last three values of a concept are given when present.

We evaluated three instruction-tuned LLM embedding models, Qwen3-Embedding-8B (Qwen3-Emb-8B) [38, 43], GTE-Qwen2-7B-Instruct (Qwen2-Emb-7B) [37, 42], and LLM2Vec-Llama-3.1-8B-Instruct (Llama3.1-LLM2Vec-8B) [39, 48], with a primary focus on the first model due to its recency. We used task-specific prompts (e.g., “Given a patient’s electronic healthcare record (EHR) in Markdown format, retrieve relevant passages that answer the query: has the patient anemia”, see Table 9). Our primary objective was to assess how general-purpose LLM-based embedding models, trained on public text data, perform in encoding EHRs for clinical prediction tasks. For comparison, we included CLMBR-T-Base, a 141-million-parameter autoregressive foundation model trained on 2.57 million de-identified EHRs from Stanford Medicine [13, 44]. Since the EHRSHOT benchmark was derived from the same hospital system, CLMBR-T-Base can be considered an in-domain baseline for this benchmark. Notably, the validation and test splits of the benchmark were kept completely separate from the model pretraining (see Fig. 1 in [44]). For each model, we computed patient-level embeddings and trained a logistic regression classifier on the training split, with hyperparameters selected using a validation set. Following the EHRSHOT protocol, we used the same simple logistic-regression head for all embedding-based representations to assess embedding quality without adding classifier complexity or overfitting risk in the few-shot setting. As a baseline, we also trained a Gradient Boosted Machine (GBM) classifier on counts of medical concepts aggregated over predefined intervals before prediction, a method that has previously shown strong performance on EHR tasks [44]. To test the effect of a GBM head, we additionally trained a GBM on Qwen3-Emb-8B embeddings, which yielded worse results (see Table 11). See Section 4.4 for additional details on model architectures.

2.2 General-Purpose LLM Embeddings Rival Domain-Specific EHR Models

Using all training and validation examples, Qwen3-Emb-8B performed nearly on par with the in-domain EHR foundation model CLMBR-T-Base on EHRSHOT, with an area under the receiver operating characteristic curve (AUROC) of 0.761 (0.733–0.788) compared to 0.769 (0.746–0.792). The LLM embedding model outperformed CLMBR-T-Base in two of the four task categories: lab test result prediction and assignment of new diagnoses (see Table 3). Qwen3-Emb-8B matched or exceeded the GBM-based counts baseline, a strong model for EHR prediction tasks [12, 13]. To assess whether the models encode complementary information, we concatenated the LLM-based and CLMBR-T-Base embeddings and observed a substantial improvement to 0.784 (0.758–0.811). We also evaluated the Multiple Embedding Model for EHR (MEME), which encodes different sections of the EHR serialization separately, yielding 0.771 (0.745–0.797) for Qwen3-Emb-8B and 0.734 (0.705–0.764) for MedBERT [34]. However, MEME required eight times as many model inferences, and the overall performance of the original MedBERT model remained considerably lower than Qwen3-Emb-8B on the full EHR serialization. Smaller model variants showed decreased average AUROC: 0.739 (0.713–0.764) for Qwen3-Emb-4B and 0.722 (0.693–0.752) for Qwen3-Emb-0.6B. The best encoder-only language models were BERT variants pretrained on medical data. Nevertheless, they performed considerably

Table 3 Performance for All Examples on EHRSHOT. Mean area under the receiver operating characteristic curve (AUROC) performance and bootstrapped 95% confidence intervals of selected models for four task groups. The macro-averaged performance across all task groups is given in the right-most column. The LLM embedding model Qwen3-Emb-8B with a context size of 8,192 tokens and a logistic regression (LR) classification head performs only slightly worse than the EHR foundation model CLMBR-T-Base, but outperforms the count-based baseline using a Gradient Boosted Machine (GBM) head. Combining the embeddings of the LLM embedding model and CLMBR-T-Base by concatenation leads to an increase in performance. Additional model variants can be found in Table 10.

Model	Operational Outcomes	Anticipating Lab Test Results	Assignment of New Diagnosis	Anticipating Chest X-ray Findings	Macro Avg. Across Task Groups
Baselines [44]					
CLMBR-T-Base	0.824 .803- .845	0.832 .824- .840	0.707 .667- .746	0.713 .702- .724	0.769 .746- .792
Count-based + GBM	0.774 .752- .797	0.728 .716- .741	0.719 .669- .768	0.656 .641- .671	0.719 .691- .748
LLM Embedding Models					
Qwen3-Emb-8B	0.776 .753- .800	0.859 .852- .866	0.717 .669- .765	0.691 .678- .704	0.761 .733- .788
Qwen3-Emb-4B	0.754 .729- .780	0.856 .849- .864	0.654 .612- .696	0.690 .678- .702	0.739 .713- .764
Qwen3-Emb-0.6B	0.749 .723- .775	0.800 .790- .810	0.683 .633- .733	0.656 .643- .669	0.722 .693- .752
LLM Embedding Model + EHR Foundation Model [44]					
Qwen3-Emb-8B + CLMBR-T-Base	0.812 .791- .833	0.880 .874- .886	0.728 .682- .775	0.717 .705- .728	0.784 .758- .811
Multiple Embedding Model for EHR (MEME) [34] with Linear Head					
Qwen3-Emb-8B MEME	0.786 .763- .810	0.882 .876- .888	0.735 .690- .780	0.680 .667- .692	0.771 .745- .797
MedBERT MEME	0.752 .730- .775	0.840 .832- .849	0.697 .645- .748	0.648 .633- .663	0.734 .705- .764
Encoder Language Models with Chunked Inputs					
ClinicalBERT	0.740 .715- .765	0.736 .725- .748	0.703 .659- .748	0.649 .636- .663	0.707 .680- .734
MedBERT	0.730 .705- .756	0.735 .723- .747	0.661 .603- .718	0.650 .638- .663	0.694 .661- .727

worse than the LLM embedding models, with 0.707 (0.680–0.734) for ClinicalBERT and 0.694 (0.661–0.727) for MedBERT. Results for all models are provided in Table 10. We plotted parameter counts versus average performance of all language models with different sizes in Fig. 3, suggesting that the performance of the Qwen3- and Qwen2-based embedding models scales with model size. We only observe a slight performance trend for the encoder-only model DeBERTa, while for BERT the performance declines with larger models. However, these encoder-only models were applied with chunked 512-token inputs, which may have contributed to this effect (see Section 4.4). Among the evaluated models, CLMBR-T-Base remained the most parameter-efficient relative to predictive performance. Nonetheless, the LLM-based embedding models were not specifically optimized for structured EHR data, which may explain their performance differences.

On the UKB dataset, Qwen3-Emb-8B consistently outperformed CLMBR-T-Base across all three prediction task groups with an overall performance of 0.748 (0.736–0.760) compared to 0.713 (0.698–0.728) (see Table 4). The performance drop of CLMBR-T-Base was expected because UKB is out-of-domain and contains many disease codes not included in the model’s pretraining vocabulary. Of UKB’s 50,702 unique medical codes, only 7,969 (16%) mapped to CLMBR’s fixed vocabulary of 26,249 codes. Consequently, 84% of codes and their associated clinical signal were

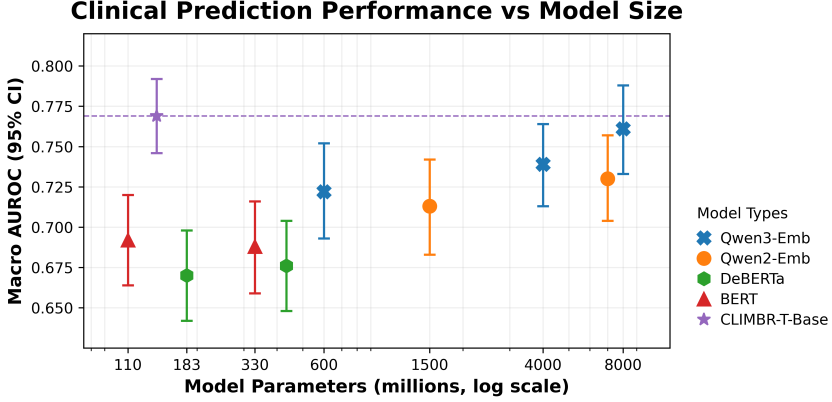


Fig. 3 Scaling Behavior on EHRSHOT. Number of model parameters (x-axis) and macro-averaged area under the receiver operating characteristic curve (AUROC) performance with bootstrapped 95% confidence intervals across all four task groups (y-axis). We include only models with varying sizes. The performance results of Qwen3- and Qwen2-based LLM embedding models suggest a scaling behavior with model size. Encoder-only models based on the BERT architecture do not show this trend. The specialized EHR foundation model, CLIMBR-T-Base, is the most parameter-efficient model. Full results in Table 10.

Table 4 Performance for All Examples on UKB. Mean area under the receiver operating characteristic curve (AUROC) performance and bootstrapped 95% confidence intervals for three task groups. The LLM embedding model Qwen3-Emb-8B with a logistic regression (LR) classification head outperforms the EHR foundation model CLIMBR-T-Base and the count-based baseline using a Gradient Boosted Machine (GBM) head. The assignment of new diagnoses prediction is based on the mean of all 23 provided diseases. Additional model variants can be found in Table 15.

Model	Mortality prediction	Operational Outcomes (Hospitalization)	Assignment of New Diagnoses	Macro Avg. Across Task Groups
Baselines [44]				
CLIMBR-T-Base	0.797 .779-.814	0.640 .628-.653	0.702 .687-.717	0.713 .698-.728
Count-based + GBM	0.738 .716-.760	0.627 .620-.635	0.699 .677-.721	0.688 .671-.705
LLM Embedding Model				
Qwen3-Emb-8B	0.840 .822-.858	0.673 .671-.675	0.732 .716-.748	0.748 .736-.760

effectively invisible to CLIMBR-T-Base. We applied careful Observational Medical Outcomes Partnership (OMOP) concept mapping to maximize coverage, but fundamental vocabulary constraints remained. In contrast, the LLM-based approaches can utilize all 50,702 codes by mapping each to a natural-language description during serialization. This ability to incorporate any code with a semantic description, without retraining, is a practical advantage for cross-institution deployment where coding practices vary substantially.

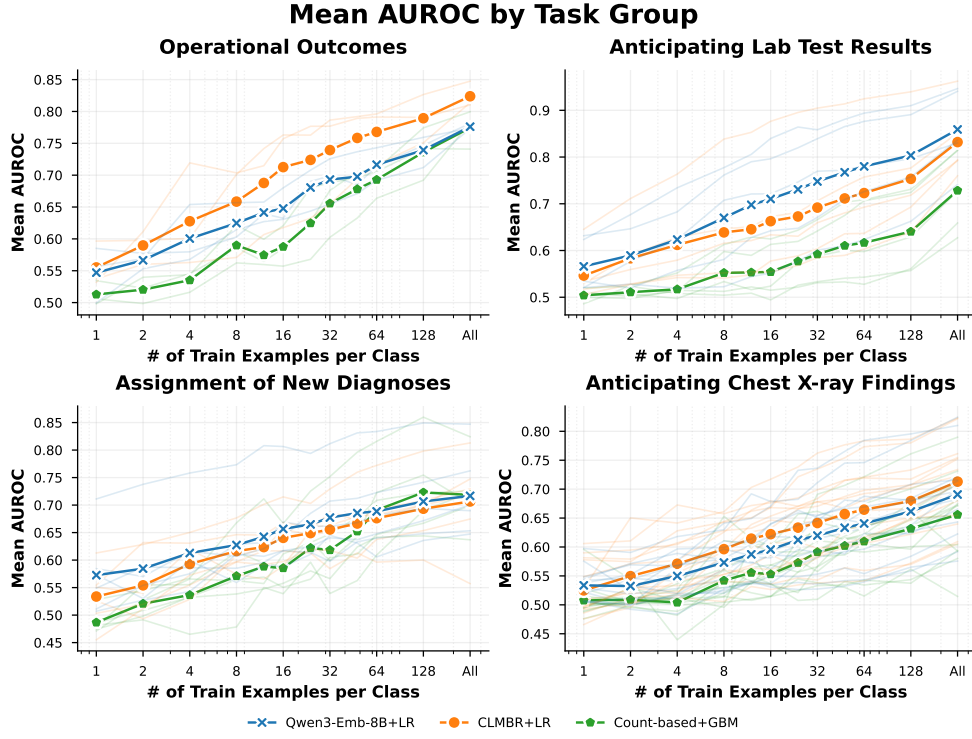


Fig. 4 Few-Shot Performance on EHRSHOT. Mean area under the receiver operating characteristic curve (AUROC) performance across subtasks for four task groups (bold). Blurred lines are averaged AUROC values across five bootstrapped runs using different seeds [44]. Similar to the EHR foundation model, CLMBR-T-Base, the LLM embedding models show the largest performance gains over the count-based model at intermediate numbers of training examples. With an increased number of training examples, the advantage of pretrained LLM-based models decreases.

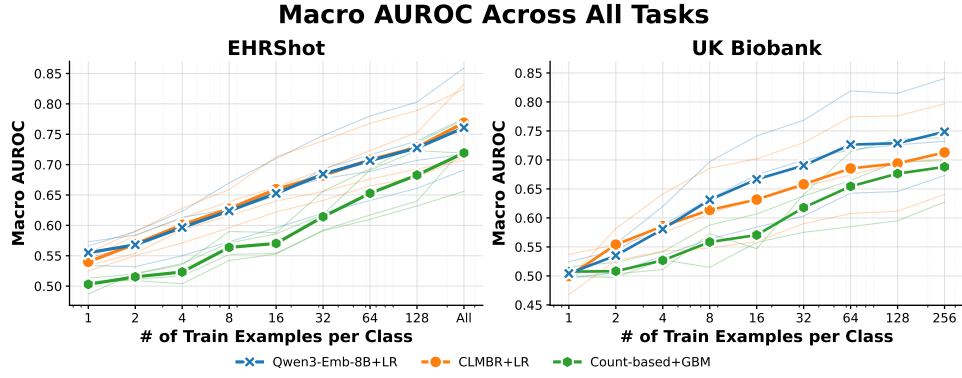


Fig. 5 Few-Shot Performance on EHRSHOT and UKB. Macro-averaged area under the receiver operating characteristic curve (AUROC) performance across all subtasks of EHRSHOT (left) and UK Biobank (right). Blurred lines show averaged AUROC values for the different task groups.

2.3 LLM Embeddings Achieve Strong Performance in Low-Data Regimes

To evaluate model performance with limited training data, we conducted experiments in a few-shot setting using small numbers of training examples. The experiments followed the EHRSHOT task definitions [44]. Fig. 4 illustrates the aggregated AUROC across all subtasks within the four task categories for varying numbers of training examples. The LLM embedding model performed strongly in the few-shot setting, suggesting effective transfer from general text pretraining to serialized EHR data. Notably, Qwen3-Emb-8B consistently outperformed CLMBR-T-Base across all training sizes for lab-test result prediction and assignment of new diagnoses. The strong results for lab-test predictions indicate that inclusion of the last three lab values in the EHR serialization provided highly predictive features, which Qwen3-Emb-8B effectively encoded. Additionally, Qwen3-Emb-8B consistently outperformed the count-based baseline across most configurations, underscoring the benefits of extensive pretraining. Consistent with previous findings [44], the largest performance improvements over the baseline were observed at intermediate training set sizes. As the number of labeled data samples increased, the relative advantage of pretrained LLM-based models diminished, highlighting the reduced marginal gains of foundation models in high-data regimes. The area under the precision-recall curve (AUPRC) results are shown in Fig. 9, with task-specific AUROC and AUPRC results provided in Fig. 10 and Fig. 11 in the Appendix.

In contrast to EHRSHOT, the LLM-based method outperformed CLMBR-T-Base in most prediction tasks on the UKB dataset. For the assignment of new diagnoses, which includes 23 tasks, Qwen3-Emb-8B outperformed CLMBR-T-Base across all sample sizes larger than two (see Fig. 12 in the Appendix). For mortality prediction and operational outcomes, CLMBR-T-Base showed stronger performance in the very low-data regime of up to four training samples. However, with more samples the performance of the LLM embedding models increased, and Qwen3-Emb-8B outperformed CLMBR-T-Base. Figure 5 presents the AUROC across all task groups for both EHRSHOT and UKB, highlighting the observed differences. On EHRSHOT, Qwen3-Emb-8B generally matched CLMBR-T-Base in performance and consistently outperformed the count-based baseline. On the UKB dataset, the LLM-based model and CLMBR-T-Base performed comparably with very limited training data of up to four examples. With additional training data, Qwen3-Emb-8B consistently outperformed CLMBR-T-Base. These findings underscore the capability of general-purpose LLM embeddings to rival or exceed the performance of domain-specific models, particularly in settings characterized by domain shift or limited labeled data. Detailed task-specific results are available in Fig. 14 and Fig. 15 in the Appendix.

2.4 Effect of the EHR Serialization on LLM-Based Embedding Performance

To assess the impact of our hand-crafted EHR serialization, we compared it with a very simple newline-separated event list ordered from most recent to oldest, with and without timestamps. Overall performance decreased only slightly from 0.761

Table 5 Performance for All Examples on EHRSHOT for Different Serializations. Area under the receiver operating characteristic curve (AUROC) performance and bootstrapped 95% confidence intervals of the Markdown EHR serialization used in this work and three data formats with little variation in performance. An alternative EHR serialization containing all events as a newline separated list ordered by recency with or without timestamps performs similar to our serialization. Additional serializations can be found in Table 11.

Model	Operational Outcomes	Anticipating Lab Test Results	Assignment of New Diagnosis	Anticipating Chest X-ray Findings	Macro Avg. Across Task Groups
EHR Serialization Formats					
Markdown (ours)	0.776 .753-.800	0.859 .852-.866	0.717 .669-.765	0.691 .678-.704	0.761 .733-.788
List events	0.799 .776-.822	0.756 .745-.767	0.727 .692-.762	0.721 .710-.732	0.751 .728-.773
List events with time	0.798 .776-.820	0.753 .742-.764	0.730 .687-.773	0.724 .712-.735	0.751 .726-.776
JSON	0.774 .750-.797	0.857 .850-.864	0.710 .669-.751	0.690 .676-.703	0.758 .733-.783
XML	0.764 .740-.789	0.863 .856-.870	0.712 .670-.755	0.682 .669-.696	0.755 .730-.781
YAML	0.775 .751-.799	0.861 .854-.868	0.722 .675-.768	0.687 .674-.701	0.761 .734-.789

(0.733–0.788) to 0.751 (0.728–0.773) (with timestamps) and 0.751 (0.726–0.776) (without timestamps). Task-group performance shifted, with gains for operational outcomes, assignment of new diagnoses, and chest X-ray findings, likely reflecting different information prioritization in the serialization. Thus, while a hand-crafted format is beneficial, the embedding method is not highly sensitive to very simple data formats. Two variants with reversed ordering performed substantially worse (see Table 11). Replacing Markdown with JSON, XML, or YAML yielded minimal differences (see Table 5). XML showed the largest decrease, which might be due to its greater formatting overhead reducing effective clinical content.

We further quantified the contribution of individual serialization components with ablations using the Qwen3-Emb-8B model (see Fig. 6 and Table 12). For these runs we used a 4,096-token limit due to computational constraints. Replacing task-specific instructions with a generic prompt slightly reduced performance, and removing instructions led to a further decrease. The largest performance drop was observed for lab-test prediction, indicating that task-aligned instructions help the model attend to relevant spans.

Removing individual components from the full serialization generally had modest effects, suggesting redundancy across data sources. A notable exception was aggregated lab results, whose removal caused a large drop in lab-test prediction from 0.866 (0.859–0.873) to 0.719 (0.706–0.731), underscoring dependence on recent lab results. Interestingly, assignment-of-new-diagnoses performance improved when condition histories were omitted, driven primarily by celiac disease (0.630 to 0.734) and lupus (0.680 to 0.743), suggesting that long lists of past diagnoses can add noise for difficult-to-ascertain or miscoded conditions.

In serializations consisting of a single component, no component matched the full EHR, underscoring the value of combining modalities. The strongest single component was conditions, achieving an AUROC of 0.707 (0.679–0.736), followed by lab results, medications, and procedures. For lab-test prediction specifically, a lab-only serialization outperformed the full EHR, likely because unrelated context was reduced. Demographics, body metrics, vital signs, and visits yielded much lower overall macro

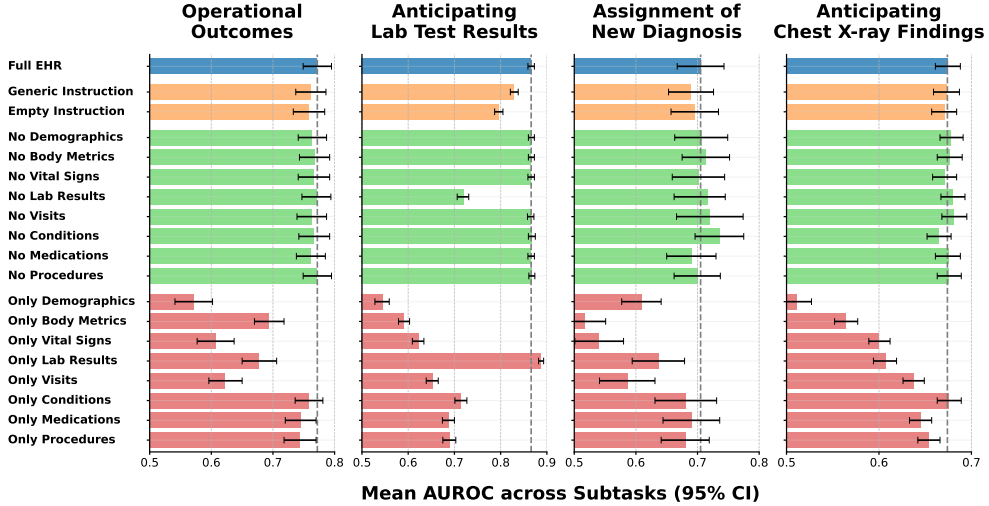


Fig. 6 Effects of EHR Serialization Components on EHRSHOT. Mean area under the receiver operating characteristic curve (AUROC) performance and bootstrapped 95% confidence intervals for Qwen3-Emb-8B using a 4,096-token limit imposed by computational constraints. The default Markdown EHR serialization (Full EHR) appears at the top, followed by runs with a generic and an empty instruction (orange). We then evaluate the serialization by removing specific components (green) and by retaining only individual components (red). Full results are reported in Table 12.

performance (see Table 12). Yet, each showed task-specific utility: demographics aided new-diagnosis assignment, body metrics supported operational outcomes, and vital signs and visits were more informative for chest X-ray findings (see Fig. 6).

2.5 Effect of Context Length and Temporal Scope on Embedding Effectiveness

To assess model sensitivity to input length and recency, we performed ablation studies on temporal window and context size using EHRSHOT data (see Fig. 7 and Table 13). The models differed in optimal context sizes, ranging from 8,192 tokens for Qwen3-Emb-8B, 4,096 for Qwen2-Emb-7B, and 2,048 for Llama3.1-LLM2Vec-8B. This pattern suggests that newer LLM embedding architectures are better able to handle longer contexts. All models exhibited sharp performance drops at 512 tokens, a common constraint in older language models [49]. All LLM embedding models improved when restricted to more recent data, with the 1-month window outperforming longer histories. Qwen3-Emb-8B and Qwen2-Emb-7B even slightly outperformed CLMBR-T-Base with a macro-AUROC of 0.773 (0.746–0.800) and 0.773 (0.746–0.801) (see Table 14) compared to 0.769 (0.746–0.792) for CLMBR-T-Base using the full data (see Table 3). Because CLMBR-T-Base is restricted to 496 input codes, it effectively encodes a limited time horizon. To disentangle long-context capacity from effects of time windows, we additionally evaluated the count-based baseline across the same temporal windows. It followed the same recency trend, indicating an inherent difficulty in performing prediction with historic data in the EHRSHOT benchmark. Using data from the day

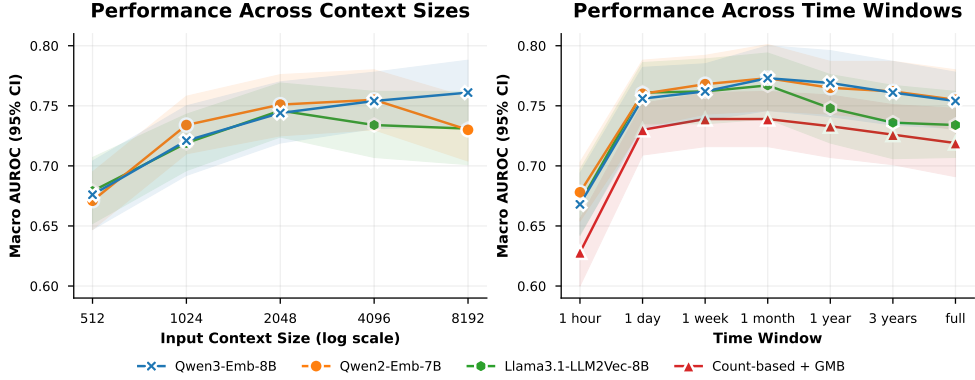


Fig. 7 Performance Across Context Size and Time Windows on EHRSHOT. Macro-averaged area under the receiver operating characteristic curve (AUROC) performance (y-axis) across all task groups for different LLM embedding models and the count-based baseline, shown for different context sizes (left) and different time windows before prediction time (right). The LLM embedding models for the time window experiments use a context size of 4,096 tokens. We do not include the count-based baseline for the context size experiments since the conversion from EHR serialization to counts is ambiguous. All results are given in Table 13 and Table 14.

before prediction remained strong across methods, whereas restricting to the last hour led to a pronounced decline.

2.6 Fine-Tuned LLM Embedding and LLM Decoder Models

To further contextualize the use of general-purpose LLMs for clinical prediction, we evaluate decoder-style LLMs that generate text, where token probabilities can be used for classification. We extend the prompt with an additional instruction to produce Yes and No tokens leveraged for prediction (see Table 9). Because of the length of the serialized EHRs, in-context few-shot prompting was infeasible, and the decoder was evaluated only in the zero-shot prompting setting. In addition, we fine-tuned both the LLM embedding model and the decoder using Low-Rank Adaptation (LoRA). The decoder experiments train the instruction-tuned causal language model Qwen3-8B to generate direct Yes and No predictions for each serialized EHR, while the encoder experiments pair Qwen3-Emb-8B with a supervised classification head (see Section 4.6). Both approaches preserve the EHRSHOT task definitions, operate on identical Markdown-based EHR serializations, and employ the same few-shot sampling strategy across all shot sizes and replicates. Due to computational constraints, we used a token limit of 4,096 tokens, and for the Anticipating Lab Test Results task group we only used a uniformly random subset of 4,096 test samples.

The zero-shot Qwen3-8B decoder achieves a macro-AUROC of 0.651 (0.593–0.707), outperforming all other model variants for up to eight training examples per class (see Fig. 8). This pattern reflects architectural differences between the two approaches: the decoder can directly exploit pretrained logits for Yes and No tokens, whereas embedding variants must learn a classification head from minimal supervision. At $k \geq$

Macro AUROC Across EHRSHOT Task Groups

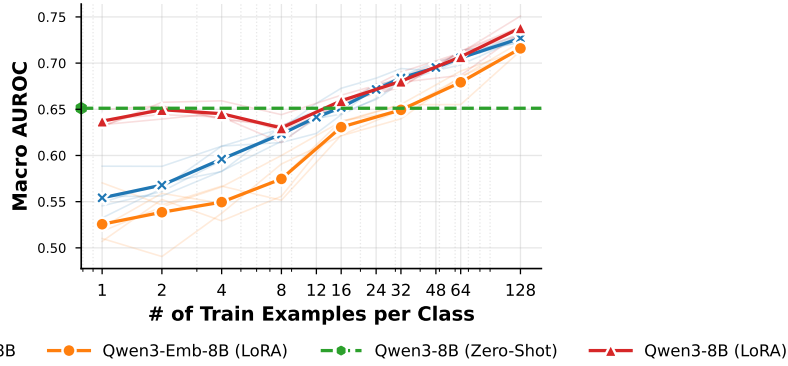


Fig. 8 Few-Shot Performance of Encoder and Decoder Models on EHRSHOT. Macro-averaged area under the receiver operating characteristic curve (AUROC) performance across all subtasks of EHRSHOT for zero to 128 training examples per class. Qwen3-Emb-8B is the encoder model used in this work (blue). We also tested a version fine-tuned end-to-end with LoRA (orange). Qwen3-8B is the decoder model with Yes and No tokens used for prediction. The decoder model is evaluated zero-shot (green) and after LoRA fine-tuning (red).

Table 6 Performance for All Examples on EHRSHOT for Encoder and Decoder Models.

Area under the receiver operating characteristic curve (AUROC) performance and bootstrapped 95% confidence intervals for LLM embedding model and decoder variant Qwen3-8B at $k = 128$. Both model variants were also fine-tuned via low-rank adaption (LoRA). Fine-tuning via LoRA does not lead to an improvement for the LLM embedding model Qwen3-Emb compared to only tuning the prediction head. For the decoder, the fine-tuned Qwen3-8B slightly outperforms Qwen3-Emb-8B, but for a much higher computational cost.

Model	Operational Outcomes	Anticipating Lab Test Results	Assignment of New Diagnoses	Anticipating Chest X-ray Findings	Macro Avg. Across Task Groups
Encoder models					
Qwen3-Emb-8B	0.739 ^{.698–.777}	0.803 ^{.785–.821}	0.706 ^{.610–.796}	0.660 ^{.612–.704}	0.727 ^{.676–.775}
Qwen3-Emb-8B (LoRA)	0.707 ^{.662–.749}	0.832 ^{.794–.868}	0.705 ^{.607–.791}	0.619 ^{.562–.674}	0.716 ^{.657–.770}
Decoder models					
Qwen3-8B (Zero-Shot)	0.583 ^{.536–.632}	0.819 ^{.780–.856}	0.645 ^{.552–.729}	0.557 ^{.503–.612}	0.651 ^{.593–.707}
Qwen3-8B (LoRA)	0.721 ^{.678–.761}	0.856 ^{.820–.888}	0.734 ^{.646–.810}	0.642 ^{.590–.692}	0.738 ^{.684–.788}

16, the fine-tuned decoder surpasses its zero-shot counterpart (0.659 (0.603–0.714)) and continues to improve with additional data (0.707 (0.653–0.758) at $k = 64$, 0.738 (0.684–0.788) at $k = 128$).

The encoder-based LLM embedding model exhibits a complementary trade-off. Fine-tuning Qwen3-Emb-8B yields steady improvements (0.526 (0.461–0.590) at $k = 1$ to 0.716 (0.657–0.770) at $k = 128$), yet the LoRA-tuned encoder consistently underperforms the frozen-encoder baseline reported in the main results across all shot sizes. We expect that larger shot counts or refined hyperparameters could narrow this gap, though computational limits precluded exploration of higher k or extensive hyperparameter sweeps. At $k = 128$, the fully fine-tuned Qwen3-8B decoder achieves a

macro-AUROC of 0.738 (0.684–0.788), marginally exceeding the fine-tuned embedding model (0.727 (0.676–0.775)), but this modest gain comes at substantially higher optimization and inference costs.

3 Discussion

Our study shows that general-purpose LLM embedding models, pretrained on large-scale natural language corpora, can be effectively repurposed for clinical prediction using EHR data. The model Qwen3-Emb-8B outperformed a strong count-based baseline and, in several clinical domains, matched or surpassed the dedicated EHR foundation model CLMBR-T-Base [13, 44]. This is notable given that CLMBR-T-Base was trained on data from the same health system as EHRSHOT. Beyond in-domain performance, the strong results on the UKB dataset highlight the generalization capabilities of LLM-based encoders under population and coding shifts. Across a broad set of tasks, including few-shot settings, our findings indicate that knowledge acquired during large-scale text pretraining enables LLMs to extract clinically meaningful patterns from serialized EHRs. Performance scaled with model size and newer architectures, suggesting further gains are likely with future LLM development. In contrast, domain-specific EHR models remain constrained by the scarcity and fragmentation of large, diverse clinical datasets. Overall, these results support general-purpose LLMs as scalable, adaptable, and high-performing alternatives for EHR representation and clinical prediction.

Our experiments suggest several key factors contribute to the success of LLM embedding models for encoding EHR data. First, task-specific instructions prepended to the EHR serialization improved performance, especially for targets that require focusing on particular spans such as lab results, aligning with the instruction-tuned nature of modern embedding models [39, 42]. Second, aggregating time series data was critical: removing aggregated laboratory values produced a large drop for lab-test prediction, underscoring the relevance of temporally proximate quantitative measurements. At the same time, the approach was robust to the choice of serialization: a very simple newline-separated event list performed only slightly worse than our hand-crafted Markdown serialization. Also, alternative data formats such as JSON and YAML showed comparable results, suggesting that model capacity rather than markup specifics drives most of the prediction performance. Third, temporal scope and context length mattered. Intermediate time windows, for example one month prior to prediction, were consistently optimal across models, indicating that recent history carries disproportionate predictive value. Long input contexts of up to 8,192 tokens could only be used effectively by Qwen3-Emb-8B, while older LLM embedding models showed a decrease in performance. Finally, we observed practical trade-offs between single-embedding serializations and multi-embedding variants like MEME [34]. While MEME produced modest average gains for Qwen3-Emb-8B on EHRSHOT, it required roughly eight times more model inferences, raising cost and latency considerations in practice.

Unlike count-based models and specialized EHR foundation models, LLM-based methods are agnostic to coding systems and data formats. Traditional EHR models rely on predefined vocabularies such as SNOMED, LOINC, and ICD, which can limit applicability across healthcare settings. For instance, CLMBR-T-Base processes 26,249 unique codes, selected from EHRSHOT [44]. When applying CLMBR-T-Base to UKB, only 7,969 of 50,702 unique codes, 16%, mapped to this fixed vocabulary, rendering most codes invisible at inference. In contrast, LLM encoders operate on text, allowing any clinical code to be incorporated via a human-readable description at serialization time. This flexibility directly addresses interoperability challenges arising from site-specific coding practices and privacy constraints that hinder pooled pretraining [50]. Moreover, broad text pretraining, often including biomedical sources, helps capture the semantics of rare or underrepresented concepts [45], mitigating the bias of count-based approaches that downweight infrequent events [51]. The same textual interface naturally supports future multimodal extensions that integrate notes, diagnostic reports, and imaging metadata [52].

Our findings highlight that LLM embedding methods combine the strengths of count-based models, specialized EHR models, and the generalization capabilities of LLMs. Count-based and specialized EHR foundation models can yield well-calibrated probabilities but are constrained by fixed vocabularies and local training distributions. Pure generation with LLMs can struggle with grounding and calibration [26]. Embedding-based pipelines bridge this gap: they leverage the representational power of LLMs while remaining compatible with standard discriminative heads such as logistic regression. This approach retains familiar calibration workflows and enables straightforward ensembling with domain-specific representations, as shown by the Qwen3-Emb-8B + CLMBR-T-Base concatenation.

We compared frozen LLM embeddings, a decoder-style LLM that directly emits **Yes** and **No** tokens, and parameter-efficiently fine-tuned variants of both. Two key observations emerged. First, the zero-shot decoder approach was competitive in the very low-shot regime for up to eight training examples even without task-specific training, likely because pretrained logits for **Yes** and **No** tokens can be exploited immediately. With more supervision for $k \geq 16$, LoRA-tuned decoding further improved, reaching a macro-AUROC of 0.738 at $k = 128$. Second, end-to-end LoRA fine-tuning of Qwen3-Emb-8B with a linear head produced steady gains with increasing k , but did not surpass the frozen-encoder baseline within the explored budgets. This supports using a frozen embedding model with a tunable classification head for LLM embedding-based EHR prediction [44]. Leveraging token outputs from decoder-style LLMs can be a viable alternative when a single, well-defined task justifies the higher training and inference costs, or when strong very-few-shot performance is required but in-context examples are infeasible due to long inputs.

This study has several limitations. First, our approach relies on a manually designed EHR serialization designed to capture medically relevant information; while ablations suggest the method is robust to simpler formats, hand-crafted choices can still introduce bias relative to models trained on raw, structured data. Second, LLM embedding model performance is sensitive to the specific content and instructions in the serialized text, which may limit reproducibility and generalization. Third, LLM

encoders have larger computational footprints than CLMBR-T-Base for population-scale screening, and many analyses were constrained to 4,096–8,192 tokens for runtime reasons, potentially excluding long-term history. Fourth, we evaluated two large cohorts, EHRSHOT and UKB; broader external validation, including settings with different documentation practices, laboratory availability, and care pathways, will be necessary to assess generalizability, calibration, and fairness at scale. Finally, while our decoder experiments provide a complementary perspective, we did not exhaust the fine-tuning design space, for example data scaling, multi-task objectives, pooling strategies, or calibration tuning, and in-context learning was impractical because serialized EHRs typically filled the context window.

Future research should explore serialization-free approaches that allow LLMs to process raw EHR tables and timelines, reducing bias from manual text transformation. Improved pooling or attention-on-attention mechanisms over long inputs may preserve salient signals without diluting them at extreme context lengths. Extending the effective context window beyond 8,192 tokens will be important for capturing comprehensive patient histories. Additionally, developing techniques to distill large LLMs into smaller, more efficient models could improve their practical use in clinical settings. Finally, expanding evaluations to real-world deployments and investigating how to combine the complementary strengths of domain-specific EHR models and general-purpose LLMs will be essential for building robust, scalable EHR foundation models.

4 Methods

4.1 EHRSHOT Database and Prediction Task

The EHR data used in our experiments is from the EHRSHOT benchmark for few-shot evaluation of EHR foundation models [44]. We obtained version 2.1 of the dataset, which is accessible via gated access under a research data use agreement. This dataset comprises longitudinal records for 6,739 patients, 921,499 visits, and 41,661,637 clinical events collected between 1990 and February 8, 2023. Each clinical event is linked to a specific patient and includes information such as start time, end time, a semantic code, a value, unit, visit ID, and the corresponding OMOP source table. We used the official ehrshot-benchmark repository¹ as a starting point to design our experiments, enabling us to build on existing functionalities and to facilitate comparisons with prior methods. The benchmark uses the Framework for Electronic Medical Records (FEMR)², which provides Python classes for efficient loading and processing of EHR data. All extensions and experiments conducted for this paper are publicly available via our GitHub repository: <https://github.com/stefanhgm/ehrshot-benchmark>. The EHRSHOT benchmark defines a rigorous evaluation including 15 clinical prediction tasks categorized into four groups: operational outcomes, anticipating lab-test results, assignment of new diagnoses, and anticipating chest X-ray findings [44]. Task labels are derived from clinical events, so a single patient can contribute multiple labels per task, resulting in substantial variation in task-specific sample sizes. For instance,

¹GitHub repository: <https://github.com/som-shahlab/ehrshot-benchmark>

²GitHub repository: <https://github.com/som-shahlab/femr>

frequent events like laboratory tests yield many more examples than rarer events such as incident diagnoses. The benchmark focuses on analyzing model performance in a few-shot setting, which is particularly relevant for large pretrained foundation models [14]. Specifically, for $k \in \{1, 2, 4, 8, 12, 16, 24, 32, 48, 64, 128\}$, the protocol uses k positive and k negative training examples and k positive and k negative validation examples to train and tune supervised classifiers. Testing is always performed on the full set of available examples for each task. The classifiers evaluated within the EHRSHOT framework include logistic regression, random forests, and GBMs [53]. Performance is reported using the AUROC and the AUPRC. For few-shot settings, we average the results over five runs with different seeds and compute bootstrapped 95% confidence intervals [44]. Mean averages are reported for each task group, and an overall macro average is provided across all groups.

4.2 EHR Text Serialization

To use LLM embedding models for representing EHR records, we serialized the records into a textual format agnostic to the prediction task. Following the EHRSHOT benchmark, we added all events before the label time. We limited the serialization length to 8,192 tokens (approximately 32,000 characters) due to computational constraints (see Section 4.8). Some additional experiments were conducted with a 4,096-token limit due to computational constraints. The primary goal was to create a detailed and informative serialization requiring minimal preprocessing while ensuring that medically relevant information appeared early in the text. This approach mitigated truncation risks in lengthy records, preserving critical details even when older entries were omitted. To convert the visits and clinical events in the EHRSHOT dataset into text, we used the semantic information embedded in the dataset. Each clinical event was labeled using the format “ontology/code”. EHRSHOT provided a set of prepared ontologies for resolving concept codes into their descriptions, which we incorporated. An analysis was performed to evaluate the use of these ontologies for all events of a subset of 200 patients across the task groups for operational outcomes and new diagnoses, covering 2,968 labels. We identified the following ontologies: Logical Observation Identifiers Names and Codes, SNOMED, RxNorm, CPT4, Domain, CARE_SITE, RxNorm Extension, Medicare Specialty, ICD10PCS, CMS Place of Service, Cancer Modifier, ICD9Proc, CVX, ICDO3, HCPCS, OMOP Extension, Condition Type. We excluded ontologies containing only a single value (Domain, Medicare Specialty, CMS Place of Service, OMOP Extension, and Condition Type). Codes of the ontologies CPT4, CARE_SITE, ICD10PCS, Cancer Modifier, CVX, and ICDO3 were not resolved with the provided ontologies. Cancer Modifier codes contained UICC cancer stages that we parsed manually. For CPT4, ICD10PCS, and CVX we used custom mapping files that we manually added.³ We excluded CARE_SITE and ICDO3 since we found no way to resolve these to useful descriptions.

Various approaches exist for serializing structured data, including row-by-row serialization [54], template-based methods [55], or structured data formats like JSON,

³We downloaded CPT4 from <https://gist.github.com/lieldulev/439793dc3c5a6613b661c33d71fdd185>, ICD10PCS from https://hcup-us.ahrq.gov/toolssoftware/procedureicd10/procedure_icd10_archive.jsp, and CVX from <https://www2a.cdc.gov/vaccines/iis/iisstandards/vaccines.asp?rpt=cvx>.

HTML, and Markdown [56]. We used Markdown due to its minimal overhead and overall benefits of using a structured data input format for LLMs [57]. To standardize temporal information, all dates were normalized relative to January 1, 2024, the prediction reference time. Only past visit dates were included, as they were considered most relevant and helped keep the serialization concise. To highlight temporal proximity, each date was annotated with the number of days before the prediction time. Serialization began with patient demographics, typically the first event for each patient, where birthdates were converted into ages (in years) for simplicity. Since 65% of the dataset comprised time-series data encoded via LOINC, which we found to be imbalanced, we aggregated LOINC-coded events. Using the same patient subset as the ontology analysis, we identified the most frequent codes and categorized them into vital signs, body metrics, and lab values, selecting 24 key medical concepts. To avoid duplicates, we merged synonymous codes (see Table 8). The last three values of each concept are presented, and we filtered implausible values. To further enrich the text representation, we manually added default units and assessments (low, normal, high) based on standard ranges (see Table 8). Following the aggregated data, a summary of all visits was included to address the potential truncation of older visits. Events not associated with visits were then presented, using the same aggregation logic to display the last three values where applicable. Finally, a detailed reverse-chronological presentation of all visits was included, with events categorized into conditions (SNOMED, Visit, Cancer Modifier, CVX, HCPCS), medications (RxNorm, RxNorm Extension), and procedures (CPT4, ICD10PCS, ICD9Proc).

4.3 Testing Alternative EHR Text Serializations

Our EHR text serialization contained several design choices and may lack generalizability. Specifically, we knew the EHRSHOT prediction tasks before designing the serialization, which could have introduced bias in the design of the EHR serialization. In total, we initially evaluated three targeted alternatives with a 4,096-token limit due to computational constraints: (1) appending a list of all unique conditions at the beginning, (2) omitting the three values for the listed concepts (e.g., for “Cigarette consumption” and “pH measurement, venous” in Fig. 2), and (3) combining both approaches. We chose the current serialization due to initial experiments with Qwen2-Emb-7B and Llama3.1-LLM2Vec-8B, where it performed on par or better than the three alternatives. To test the effect of our serialization format more broadly, we also evaluated a very simple serialization by creating a newline-separated list of all medical events of a patient ordered by time. We tested four variants with different sorting directions and with and without timestamps.

Additionally, we tested three data formats by converting the structured Markdown serialization into JSON, XML, and YAML. We used standard Python libraries for the conversion process. Due to different formatting overheads of the formats, the amount of clinical content included under a fixed token budget may differ.

4.4 LLM Embedding Models and Baselines

We evaluated three LLM embedding models: Qwen3-Embedding-8B (Qwen3-Emb-8B) [38, 43], GTE-Qwen2-7B-Instruct (Qwen2-Emb-7B) [37, 42], and LLM2Vec-Llama-3.1-8B-Instruct (Llama3.1-LLM2Vec-8B) [39, 48], based on state-of-the-art decoder-only LLMs. We selected these models for their ability to handle the 8,192-token EHR serializations used in our experiments. For comparison, we also tested smaller variants of Qwen3-Emb-8B and Qwen2-Emb-7B. All LLM-based models received task-specific instructions prepended to the EHR serialization (see Section 4.5), and we used each model’s default embedding configuration. For Qwen-based embedding models, we used the last-layer hidden state of the final ([EOS]) token as the patient embedding [37, 43]. For LLM2Vec models, we applied mean pooling over the last-layer hidden states corresponding to the EHR serialization, excluding the instruction tokens from pooling [39]. Importantly, the instruction still conditions the internal representation and thus influences the resulting embedding.

As additional baselines, we included commonly used encoder-only embedding models with shorter input limits (512 tokens). To apply them to 8,192-token inputs, we split each input into up to 16 chunks of 512 tokens and averaged the chunk embeddings to obtain a single representation. These encoder-only models did not use task instructions, and embeddings were computed via mean pooling over the last hidden layer. Below is an overview of all models.

Qwen3-Embedding-8B/4B/0.6B

This model family is built on the Qwen3 foundation LLMs [38] and trained as instruction-aware embedding models via a multi-stage recipe [43]. All variants use decoder-only Transformers with causal attention and produce the embedding from the last-layer hidden state of the final [EOS] token (see Section 4.5). The 8B and 4B models have 36 layers, while the 0.6B model has 28 layers; all support a context window of up to 32,000 tokens. By default, the embedding dimensionality is 4,096 (8B), 2,560 (4B), and 1,024 (0.6B), with support for flexible output dimensions. Training comprises large-scale weakly supervised pretraining on synthetic query–document pairs followed by supervised fine-tuning on labeled and filtered synthetic data optimizing a contrastive learning objective. Finally, different checkpoints are merged to improve robustness [43].

Qwen2-Embedding-7B/1.5B

Built on GTE-Qwen2-7B-Instruct and GTE-Qwen2-1.5B-Instruct [37], these models use decoder-only Transformers (7B: 28 layers, 28 heads, hidden size 3,584; 1.5B: 28 layers, 12 heads, hidden size 1,536). They are first trained with autoregressive next-token prediction and then converted to embedding models via the General Text Embedding (GTE) procedure [42], which replaces the causal mask with a BERT-like bidirectional attention during embedding extraction. Contrastive learning was applied using a mixture of private datasets to enhance embedding performance. The models also incorporate instructions tailored for embedding tasks and support a context size of up to 32,000 tokens.

Llama3.1-LLM2Vec-8B

This model is built upon the Llama-3.1-8B-Instruct LLM [48], which has a decoder-only Transformer architecture with 32 layers, 32 attention heads, and a hidden size of 4,096⁴. Initially trained for next-token prediction, it was converted to an embedding model using the LLM2Vec method [39]. This method adds bidirectional attention and fine-tunes the model with supervised contrastive learning on embedding tasks. The fine-tuning used curated data from the public E5 dataset [58, 59], containing approximately 1.5 million entries. The model supports task-specific instructions and supports a context size of up to 128,000 tokens.

DeBERTa v3 base/large

DeBERTa v3 is an encoder-only Transformer model designed for token embeddings [60]. It improves upon its predecessor by replacing the masked language modeling objective with replaced token detection and using Gradient-Disentangled Embedding Sharing. We evaluated the base variant (12 layers, 12 attention heads, 768 hidden size) and the large variant (24 layers, 12 attention heads, 1,024 hidden size), with parameter counts of 183M and 434M, respectively⁵.

BERT base/large

BERT is a well-established text embedding model using an encoder-only Transformer trained with the masked language modeling objective [15]. We included both the base (12 layers, 12 attention heads, 768 hidden size, 110M parameters) and large (24 layers, 16 attention heads, 1,024 hidden size, 340M parameters) variants as benchmarks⁶. While not state-of-the-art, BERT models remain widely used in embedding tasks.

Bio_ClinicalBERT

This model builds on BERT-Base, further fine-tuned on biomedical [61] and clinical data [62]. It is a widely adopted embedding model for medical text and was included as a baseline for comparison⁷.

MedBERT

This model builds on Bio_ClinicalBERT via continued domain pretraining on heterogeneous biomedical corpora (N2C2, BioNLP, CRAFT, and biomedical Wikipedia) and was originally introduced for biomedical NER [63]. We include it as a domain-adapted baseline for comparison⁸.

CLMBR-T-Base

CLMBR-T-Base is a specialized EHR foundation model trained on 2.57 million de-identified EHRs from Stanford Medicine with autoregressive next code prediction [13, 44]. It uses transformers and has 12 layers and a hidden dimension of 768⁹. The

⁴Hugging Face identifier: McGill-NLP/LLM2Vec-Meta-Llama-31-8B-Instruct-mntp-supervised

⁵Hugging Face identifiers: microsoft/deberta-v3-base,large

⁶Hugging Face identifiers: google-bert/bert-base,large-uncased

⁷Hugging Face identifier: emilyalsentzer/Bio_ClinicalBERT

⁸Hugging Face identifier: Charangan/MedBERT

⁹Hugging Face identifier: StanfordShahLab/clmbr-t-base

model has 141M parameters and allows for a context window of 496 codes. CLMBR-T-Base has demonstrated consistent improvements over count-based baselines for a variety of clinical prediction tasks [44]. It serves as a main baseline for our experiments to test specialized EHR models against general-purpose text embedding models for representing EHR records.

LLM Embedding Model and CLMBR-T-Base

To test whether the LLM embedding models and the EHR foundation model learn orthogonal information, we combined both models for the prediction. To this end, we simply appended both embeddings. The resulting embeddings have dimensions 4,864 for Qwen3-Emb-8B.

Count-based Model

Count models have proven to be strong baselines for EHR prediction tasks [6, 12, 13]. The basic idea is to encode all EHR events of a patient in a single vector where each entry represents the number of occurrences of a medical concept. We used the count-based baseline introduced in [44], which uses counts from different time intervals and extends this approach with ontology expansion, enriching the vectors with parent and child concepts. Notably, this baseline does not incorporate any values associated with medical concepts, such as laboratory measurements, vital signs, or other continuous fields, but only the occurrence counts of each concept code.

Based on the embeddings or the counts vectors generated by the methods described above, a classification head was trained and validated for each prediction task. For the embedding models we used a logistic regression head. For the count-based model, we used a GBM [53], which proved superior [44]. We adopted the parameter tuning of the classification heads from the EHRSHOT benchmark to ensure comparability of results.

4.5 Instructions for LLM Embedding Models

The Qwen and LLM2Vec models used instruction-tuned embeddings, requiring task-specific prompts. Hence, we added simple instructions for each prediction task based on their respective instruction templates. For instance, for prediction of anemia, we added “Given a patient’s electronic healthcare record (EHR) in Markdown format, retrieve relevant passages that answer the query: has the patient anemia”. The existing EHRSHOT benchmark encoded the EHRs of the same patient and the identical prediction times only once for efficiency reasons. However, to support task-specific instructions, we changed this default behavior and encoded each (patient, task, prediction time) instance, leading to 1,161,412 instead of 406,379 EHRs to encode and resulting in longer processing times. The difference between 1,161,412 labels used in our experiments and the total number of labels of 1,178,665 (see Table 2) is because some labels share the same task and prediction time and are therefore merged. Encoder-only language models did not use instructions and thus required encoding only the 406,379 EHRs from the original implementation, yielding a substantial computational advantage. For assignment of new diagnoses tasks in UKB, the same prompt

was used for all diseases to reduce computational resources. We list all instructions in Table 9 and perform ablations to test the effect of the instructions.

4.6 Fine-Tuned LLM Embedding and LLM Decoder Models

We evaluated two approaches for clinical prediction: LLM embedding models that encode the EHR serialization into a fixed-length vector prior to classification, and LLM decoder models that generate text whose token probabilities can be used for classification. We further assessed the effect of fine-tuning for both approaches.

To this end, we implemented a pipeline for fine-tuning Qwen3-Emb-8B [38, 43] with LoRA adapters [64] applied to the encoder attention projections and MLP blocks. The encoder is wrapped in a lightweight classification head consisting of a dropout layer (dropout rate 0.1) and a linear projection. Inputs are constructed by concatenating the task instruction and the EHR serialization, tokenized with enforced left padding to preserve relative recency, and batched with a custom collator that truncates to 4,096 tokens. The entire model is optimized end-to-end with cross-entropy loss. For comparability, both the encoder and decoder variants use the same LoRA hyperparameters ($r = 16$, $\alpha = 32$, dropout 0.05). Training uses the Hugging Face `Trainer` with cosine learning-rate decay, early stopping (patience five epochs), gradient checkpointing, and gradient accumulation chosen so that all variants share an effective batch size of 8. The models are trained with mixed precision (BF16), and zero-shot runs ($k = 0$) are evaluated without parameter updates to the backbone.

The decoder pipeline adapts the instruction-tuned causal Qwen3-8B¹⁰ checkpoint [38] with LoRA adapters applied to all attention projections and MLP up/down projections (`q_proj`, `k_proj`, `v_proj`, `o_proj`, `up_proj`, `down_proj`, `gate_proj`). Serialized visits are converted into chat-formatted prompts that additional prepend task instructions enforcing the output of `Yes` or `No` tokens (see Table 9). During LoRA fine-tuning, the model is trained to predict the literal tokens `Yes` or `No` as target labels. During scoring, the model predicts token probabilities for `Yes` and `No` at the final decoding step. We aggregate probabilities across all variants of these tokens (including different capitalizations and punctuation) to yield calibrated decision scores without additional heads.

For both model families, evaluation computes AUROC, AUPRC, and Brier score on the held-out test set, alongside 1,000 patient-level bootstrap replicates to estimate standard deviations and 95% confidence intervals. To keep computational cost manageable, we used a token limit of 4,096 and evaluated the Anticipating Lab Test Results group on a uniformly random subset of 4,096 test samples in each run.

4.7 Existing Methods Using Language Models for EHR Prediction

Two broad approaches have emerged for leveraging language models with structured EHR data: using model generations directly for prediction and using vector embeddings derived from the model’s hidden states. Early work on the generation-based approach converted structured insurance claims into short text snippets and queried

¹⁰Hugging Face identifier: Qwen/Qwen3-8B

an encoder-decoder model with a 512-token context limit, reporting improvements over logistic regression in few-shot regimes (16–64 examples) for end-of-life, surgery, and length-of-stay tasks [26]. Subsequent studies explored more capable LLMs, prompt design, and fine-tuning strategies on serialized EHR inputs, generally treating prediction as text generation or calibrated scoring from logits [27–32]. One variant constrains the model’s output space to medical codes to better align free-text reasoning with code-based clinical labels, thereby bridging the gap between general-purpose language models and EHR-specific foundation models [65].

In contrast to generation, embedding-based methods treat an EHR-to-text serialization as input and extract a fixed-dimensional representation for a downstream classifier [33–35]. Gao et al. provide a systematic comparison across serialization formats, LLMs, and embedding strategies on MIMIC-III and a private 660-patient clinical-deterioration dataset, and report that LLM embeddings paired with a prediction head can be competitive in some settings. However, raw numerical features remain strong baselines [33]. They also evaluate an encoder based approach producing `Yes` and `No` tokens in the zero-shot setting but find no discriminatory abilities for Mistral-7B-Instruct and Llama3-8B-Instruct. The DeLLiriuM method introduced in [35] also evaluates embeddings derived from different LLMs for delirium prediction and performs detailed model introspection via a SHAP analysis. Most similar to our work is the Multiple Embedding Model for EHR (MEME) method, which encodes different EHR modalities such as vitals, medications, and diagnoses into separate embeddings and fuses them with a self-attention layer [34]. This framework uses the relatively small and efficient MedBERT language model for embedding creation and reports superior performance to GPT-4 [34].

Our study follows the embedding paradigm but differs from prior work in three ways. First, we use LLMs explicitly adapted for embedding via contrastive learning. Second, we operate with substantially longer inputs (up to 8,192 tokens), which is important for longitudinal EHR serialization where earlier studies often processed up to 3,076 tokens [33] or relied on chunking [34]. Third, we evaluate on large public longitudinal cohorts and standardized benchmarks from EHRSHOT and UKB. We also include a MEME-style baseline with a linear head in place of self-attention due to data sparsity [34]. Finally, consistent with [33], we explicitly compare embeddings to direct LLM outputs and examine parameter-efficient fine-tuning to assess robustness and practical trade-offs (see Section 2.6).

4.8 Computational Setup and Running Times

All experiments were conducted on the Charité High-Performance Cluster using Nvidia A100 GPUs with 80 GB memory, configured with one, four, or eight GPUs (DGX systems). Running the Qwen3-Emb-8B model with our serialization truncated at 8,192 tokens on an 8-GPU DGX system required approximately 40 hours. For the same setup Qwen2-Emb-7B required approximately 31 hours. For the Llama3.1-LLM2Vec-8B model, runtime errors occurred during multi-GPU experiments with the full dataset. These issues were resolved by splitting the data into smaller batches, which introduced additional overhead. Additionally, we optimized the LLM2Vec code by removing an initial *word-boundary token-limit routine* that iteratively re-tokenizes to ensure the

final cut occurs at a word boundary; this step took approximately eight hours when using the full data. With our workaround, inputs are simply truncated at the maximum token number (i.e., the last token may correspond to an incomplete word), which matches how the Qwen implementation handles over-length inputs. Importantly, this modification does not perform any semantic text pruning or content selection and should have only a minimal effect on performance, limited to a potentially incomplete trailing word. Using this modified setup, the Llama3.1-LLM2Vec-8B model took approximately 46 hours to complete on eight A100 GPUs. The calculation of the embeddings for the 387,464 UKB patients took approximately 80 hours on a single GPU per task for Qwen2-Emb-7B and Llama3.1-LLM2Vec-8B and approximately 100 hours for Qwen3-Emb-8B, all for a token length of 8,192. For significantly reducing the overall runtime, the calculations can be split onto separate GPUs. Additionally, since the embedding for the disease prediction task is not disease specific, for each model only three embeddings had to be calculated per patient.

4.9 Performance Results on EHRSHOT Prediction Tasks and Few-Shot Setting

Following the EHRSHOT benchmark, we evaluated all models across 15 prediction tasks under various few-shot settings. The benchmark includes a modular pipeline designed to execute key tasks, with the flexibility to optionally use a Slurm cluster for distributed execution. Running all steps within this pipeline ensures full reproducibility of results. Step four of the pipeline, which generates EHR representations with CLMBR-T-Base and the count-based model, was extended to incorporate our method for creating language model-based EHR representations. This adaptation allowed us to reuse significant portions of the existing code, including the task evaluation framework. Additionally, we implemented new functionality for EHR serialization and slightly modified other steps of the benchmark to accommodate our experimental setup. For instance, the label creation process was adjusted (step three) to enable task-specific instructions for the LLM embedding models. All modifications have been documented and can be tracked in our public GitHub repository.

4.10 External Validation on UK Biobank

External validation was performed using data from the UKB, a large-scale prospective cohort study comprising 502,489 UK participants recruited between 2006 and 2010, with a median follow-up of 13.8 years. We used linked EHR data from primary care (General Practitioner (GP)) and secondary care (Hospital Episode Statistics (HES)), providing information on diagnoses, procedures, and prescriptions.

Initial data preprocessing, including cleaning, feature extraction, missing-value imputation, and endpoint selection, followed the methodology described in [45]. All health records were mapped to the OMOP CDM using mapping tables provided by the UKB, SNOMED International, and the OHDSI community for mapping concepts from provider and country-specific non-standard vocabularies to OMOP standard vocabularies. Participants lacking any recorded GP or HES events either before or after

their recruitment date were excluded, resulting in a validation cohort of 387,464 individuals. Diagnostic codes were mapped to Phecodes X [66, 67] (derived directly from source ICD-10 or by mapping from SNOMED to ICD-10 codes and subsequently to Phecodes X) primarily for standardized endpoint definition and cohort selection. To avoid redundancy with source codes used as features, the Phecodes themselves were excluded during the creation of patient sequences for model input. Due to significant challenges in mapping and harmonizing UKB laboratory values [68], and to ensure comparability across models and tasks, laboratory data were excluded entirely, differing from the use of binary labels in [45]. The final feature set comprised conditions (SNOMED, CVX), medications (RxNorm), and procedures (SNOMED).

Given that UKB represents a general population cohort, we adjusted the proposed prediction tasks to define relevant longitudinal health trajectory tasks. These tasks included: (1) prediction of all-cause hospitalization within the next year (operational outcomes), (2) prediction of incident diagnoses for a set of selected conditions (assignment of new diagnoses), and (3) prediction of all-cause mortality (mortality prediction). The selection of incident diseases for the assignment of new diagnoses task group largely followed [45], focusing on common conditions, diseases lacking established risk stratification tools, and specific cardiovascular conditions. From the initial 24 endpoints proposed in [45], we treated all-cause mortality as a separate task. For the assignment of new diagnoses and mortality tasks, patients with a diagnosis of the respective endpoint recorded prior to their UKB recruitment date were excluded to prevent data leakage; this exclusion was not applied to the hospitalization task due to high incidence. Following task-specific exclusions, the final sample size available for analysis ranged from 300,344 to 359,250 patients, depending on the prediction task (see Table 7 for details). For all three task groups, the prediction window was set to one year after the prediction year.

The pretrained CLMBR-T-Base model operates with a fixed vocabulary of 26,249 unique codes. To use this model, we mapped the 50,702 unique medical codes (SNOMED CT, RxNorm, CVX) present in our processed UKB cohort to the CLMBR-T-Base vocabulary. This mapping followed steps similar to those implemented in the FEMR package¹¹, involving direct code matching where possible, supplemented by indirect mapping via the OHDSI ATHENA vocabulary using 'Maps to' relationships and inclusion of ancestor concepts. This process successfully mapped 7,969 unique UKB codes to the CLMBR-T-Base vocabulary (in format ontology/code), which means that the remaining codes were implicitly excluded from the input sequences for this model. After creating patient timelines, adding information about birth date, ethnicity, and visits, the data was converted into the MEDS standard [69], from which the embeddings were calculated. Additionally, UKB ethnicities were converted to the ethnicity groups used by CLMBR-T-Base. For transforming the patient information into embeddings, we mainly followed the code provided by FEMR (primarily the `convert_patient` function¹²) with minor modifications to enable batch processing.

¹¹<https://github.com/som-shahlab/femr/tree/0ebf454303091fa83c9e4023e7db9ba9b68af09a>

¹²<https://huggingface.co/StanfordShahLab/clmbr-t-base>

Similar to the approach of Wornow et al. [44], we performed an ontology expansion to improve the count-based baseline by adding direct parent and grandparent concepts. This increased the unique code count from 51,677 to 69,850, aiming to capture broader hierarchical relationships between medical concepts. However, the resulting high dimensionality posed memory challenges for a standard counts matrix. To mitigate this, we implemented feature selection by removing codes present in fewer than 50 individuals (<0.01% of the cohort), reducing the feature space to 24,509 unique codes. To ensure a more comparable baseline to the other models, which implicitly incorporate patient context, we explicitly added normalized age at prediction time and coded sex as additional features to the feature matrix used for the count-based baseline.

All approaches were evaluated using a five-fold cross-validation. Within each fold, hyperparameters were optimized on a dedicated validation set of similar sample size to that of the training partition in that fold. For each fold, patients were randomly assigned to train, validation, and test sets. The test set for each task within a fold was constructed by selecting all available positive cases (capped at 10,000), and an equal number of negative cases after allocating patients to the train and validation sets. To specifically assess performance in low-data scenarios, mimicking potential clinical applications with limited examples, we again evaluated models using incrementally larger subsets of the training data, with the final evaluation point capped at a sample size of 256 patients from the training set, even when larger test sets were available.

4.11 Ablation Studies of EHR Serialization

To better understand the contribution of various components in the EHR serialization process to the performance of the LLM embedding models, we conducted a series of ablation studies. These ablations used Qwen3-Emb-8B with a 4,096-token limit due to computational constraints. We first examined the role of task-specific instructions by replacing them with a generic prompt (see Table 9) or removing instructions entirely, thereby isolating their contribution to the resulting embeddings. Next, we systematically excluded individual elements of the serialization, demographics, body metrics, vital signs, laboratory values, visit headings, conditions, medications, and procedures, while keeping all other parts of the pipeline fixed to avoid confounding. Finally, we constructed serializations that retained only one of these components at a time to assess its standalone predictive value. Together, these experiments identify which elements are most critical for producing effective EHR representations and clarify how the models leverage structured clinical data for downstream prediction tasks.

4.12 Effect of Different Time Windows

To examine the influence of recency on predictive performance, we varied the time window preceding the prediction date used during EHR text serialization. We evaluated Qwen3-Emb-8B, Qwen2-Emb-7B, Llama3.1-LLM2Vec-8B, and the count-based baseline with a GBM head across seven intervals: one hour, one day, one week (7 days), one month (30 days), one year (365 days), three years (1,095 days), and full history. For each window, only events occurring within the specified interval before the prediction time were included. Hence, only data from the respective time window

contributed to the aggregated information and the visit data in the EHR serialization. All other aspects of the serialization, including structure, formatting, and instruction prompts remained unchanged to isolate the effect of the temporal window.

4.13 Effect of Different Context Sizes

We investigated the impact of varying context sizes in the LLM embedding models. We sought to determine whether encoding information from older visits enhances prediction performance and whether longer inputs might dilute critical details, such as laboratory values, in the final embeddings. Specifically, we evaluated Qwen3-Emb-8B, Qwen2-Emb-7B, and Llama3.1-LLM2Vec-8B models with input token limits of 512, 1,024, 2,048, 4,096 and 8,192 tokens. Input tokens exceeding these thresholds were discarded. Due to the design of our EHR serialization process, additional input tokens primarily consisted of medical concepts from past visits. All other preprocessing choices and task-specific instructions were held fixed across context-size settings. By testing these varying context sizes, we aimed to assess the balance between capturing historical medical data and preserving the clarity of high-priority information within the embeddings.

Acknowledgements

Funded by the Deutsche Forschungsgemeinschaft (DFG, German Research Foundation) – Project-ID 437531118 – SFB 1470 and German Federal Ministry of Education and Research (BMBF) Project-ID 01ZZ2317G.

Declaration of interest

The authors declare no competing interests.

Data availability

The EHRSHOT data is available through gated access via <https://doi.org/10.57761/0gv9-nd83>. UK Biobank data, including all linked routine health records, are publicly available to bona fide researchers upon application at <http://www.ukbiobank.ac.uk/using-the-resource>. In this study, only primary care data not subject to the Government’s Control of Patient Information (COPI) notice was used (UK Biobank Category 3000).

Code availability

All extensions and experiments conducted for this paper have been made publicly available via our GitHub repository: <https://github.com/stefanhgm/ehrshot-benchmark>.

References

- [1] Dash, S., Shakyawar, S.K., Sharma, M., Kaushik, S.: Big data in healthcare: management, analysis and future prospects. *Journal of Big Data* **6**(1), 54 (2019) <https://doi.org/10.1186/s40537-019-0217-0> . Accessed 2025-02-15
- [2] Ahsan, H., McInerney, D.J., Kim, J., Potter, C., Young, G., Amir, S., Wallace, B.C.: Retrieving Evidence from EHRs with LLMs: Possibilities and Challenges. *Proceedings of machine learning research* **248**, 489–505 (2024). Accessed 2025-02-15
- [3] Rajkomar, A., Dean, J., Kohane, I.: Machine Learning in Medicine. *New England Journal of Medicine* **380**(14), 1347–1358 (2019) <https://doi.org/10.1056/NEJMra1814259> . Accessed 2020-06-05
- [4] Xu, Y., Lv, T., Cui, L., Wang, G., Lu, Y., Florencio, D., Zhang, C., Wei, F.: LayoutXLM: Multimodal Pre-training for Multilingual Visually-rich Document Understanding. *arXiv. arXiv:2104.08836 [cs]* (2021). <https://doi.org/10.48550/arXiv.2104.08836> Accessed 2024-07-23
- [5] Golas, S.B., Shibahara, T., Agboola, S., Otaki, H., Sato, J., Nakae, T., Hisamitsu, T., Kojima, G., Felsted, J., Kakarmath, S., Kvedar, J., Jethwani, K.: A machine learning model to predict the risk of 30-day readmissions in patients with heart failure: a retrospective analysis of electronic medical records data. *BMC Medical Informatics and Decision Making* **18**(1), 44 (2018) <https://doi.org/10.1186/s12911-018-0620-z> . Accessed 2024-12-14
- [6] Rajkomar, A., Oren, E., Chen, K., Dai, A.M., Hajaj, N., Hardt, M., Liu, P.J., Liu, X., Marcus, J., Sun, M., Sundberg, P., Yee, H., Zhang, K., Zhang, Y., Flores, G., Duggan, G.E., Irvine, J., Le, Q., Litsch, K., Mossin, A., Tansuwan, J., Wang, D., Wexler, J., Wilson, J., Ludwig, D., Volchenboum, S.L., Chou, K., Pearson, M., Madabushi, S., Shah, N.H., Butte, A.J., Howell, M.D., Cui, C., Corrado, G.S., Dean, J.: Scalable and accurate deep learning with electronic health records. *npj Digital Medicine* **1**(1), 1–10 (2018) <https://doi.org/10.1038/s41746-018-0029-1> . Publisher: Nature Publishing Group. Accessed 2024-12-15
- [7] Lauritsen, S.M., Kalør, M.E., Kongsgaard, E.L., Lauritsen, K.M., Jørgensen, M.J., Lange, J., Thiesson, B.: Early detection of sepsis utilizing deep learning on electronic health record event sequences. *Artificial Intelligence in Medicine* **104**, 101820 (2020) <https://doi.org/10.1016/j.artmed.2020.101820> . Accessed 2024-12-15
- [8] Moor, M., Bennett, N., Plečko, D., Horn, M., Rieck, B., Meinshausen, N., Bühlmann, P., Borgwardt, K.: Predicting sepsis using deep learning across international sites: a retrospective development and validation study. *eClinicalMedicine* **62** (2023) <https://doi.org/10.1016/j.eclim.2023.102124> . Publisher: Elsevier. Accessed 2024-12-15

[9] Thorsen-Meyer, H.-C., Nielsen, A.B., Nielsen, A.P., Kaas-Hansen, B.S., Toft, P., Schierbeck, J., Strøm, T., Chmura, P.J., Heimann, M., Dybdahl, L., Spangsege, L., Hulsen, P., Belling, K., Brunak, S., Perner, A.: Dynamic and explainable machine learning prediction of mortality in patients in the intensive care unit: a retrospective study of high-frequency data in electronic patient records. *The Lancet. Digital Health* **2**(4), 179–191 (2020) [https://doi.org/10.1016/S2589-7500\(20\)30018-2](https://doi.org/10.1016/S2589-7500(20)30018-2)

[10] Desai, R.J., Wang, S.V., Vaduganathan, M., Evers, T., Schneeweiss, S.: Comparison of Machine Learning Methods With Traditional Models for Use of Administrative Claims With Electronic Medical Records to Predict Heart Failure Outcomes. *JAMA Network Open* **3**(1), 1918962 (2020) <https://doi.org/10.1001/jamanetworkopen.2019.18962> . Accessed 2024-12-15

[11] Kim, E., Rubinstein, S.M., Nead, K.T., Wojcieszynski, A.P., Gabriel, P.E., Warner, J.L.: The Evolving Use of Electronic Health Records (EHR) for Research. *Seminars in Radiation Oncology* **29**(4), 354–361 (2019) <https://doi.org/10.1016/j.semradonc.2019.05.010> . Accessed 2025-02-15

[12] Rasmy, L., Xiang, Y., Xie, Z., Tao, C., Zhi, D.: Med-BERT: pretrained contextualized embeddings on large-scale structured electronic health records for disease prediction. *npj Digital Medicine* **4**(1), 1–13 (2021) <https://doi.org/10.1038/s41746-021-00455-y> . Publisher: Nature Publishing Group. Accessed 2024-12-15

[13] Steinberg, E., Jung, K., Fries, J.A., Corbin, C.K., Pfahl, S.R., Shah, N.H.: Language models are an effective representation learning technique for electronic health record data. *Journal of Biomedical Informatics* **113**, 103637 (2021) <https://doi.org/10.1016/j.jbi.2020.103637> . Accessed 2024-06-12

[14] Bommasani, R., Hudson, D.A., Adeli, E., Altman, R., Arora, S., Arx, S.v., Bernstein, M.S., Bohg, J., Bosselut, A., Brunsell, E., Brynjolfsson, E., Buch, S., Card, D., Castellon, R., Chatterji, N., Chen, A., Creel, K., Davis, J.Q., Demszky, D., Donahue, C., Doumbouya, M., Durmus, E., Ermon, S., Etchemendy, J., Ethayarajh, K., Fei-Fei, L., Finn, C., Gale, T., Gillespie, L., Goel, K., Goodman, N., Grossman, S., Guha, N., Hashimoto, T., Henderson, P., Hewitt, J., Ho, D.E., Hong, J., Hsu, K., Huang, J., Icard, T., Jain, S., Jurafsky, D., Kalluri, P., Karamcheti, S., Keeling, G., Khani, F., Khattab, O., Koh, P.W., Krass, M., Krishna, R., Kuditipudi, R., Kumar, A., Ladhak, F., Lee, M., Lee, T., Leskovec, J., Levent, I., Li, X.L., Li, X., Ma, T., Malik, A., Manning, C.D., Mirchandani, S., Mitchell, E., Munyikwa, Z., Nair, S., Narayan, A., Narayanan, D., Newman, B., Nie, A., Niebles, J.C., Nilforoshan, H., Nyarko, J., Ogut, G., Orr, L., Papadimitriou, I., Park, J.S., Piech, C., Portelance, E., Potts, C., Raghunathan, A., Reich, R., Ren, H., Rong, F., Roohani, Y., Ruiz, C., Ryan, J., Ré, C., Sadigh, D., Sagawa, S., Santhanam, K., Shih, A., Srinivasan, K., Tamkin, A., Taori, R., Thomas, A.W., Tramèr, F., Wang, R.E., Wang, W., Wu, B., Wu, J., Wu, Y., Xie, S.M., Yasunaga, M., You, J., Zaharia, M., Zhang, M., Zhang, T., Zhang, X., Zhang, Y., Zheng,

L., Zhou, K., Liang, P.: On the Opportunities and Risks of Foundation Models. arXiv. arXiv:2108.07258 [cs] (2022). <https://doi.org/10.48550/arXiv.2108.07258> . <http://arxiv.org/abs/2108.07258> Accessed 2024-12-16

[15] Devlin, J., Chang, M.-W., Lee, K., Toutanova, K.: BERT: Pre-training of Deep Bidirectional Transformers for Language Understanding. Proceedings of the 2019 Conference of the North American Chapter of the Association for Computational Linguistics: Human Language Technologies, Volume 1 (Long and Short Papers), 4171–4186 (2019) <https://doi.org/10.18653/v1/N19-1423> . Accessed 2022-04-22

[16] Radford, A., Wu, J., Child, R., Luan, D., Amodei, D., Sutskever, I.: Language Models are Unsupervised Multitask Learners. Technical report, OpenAi, 24 (2019)

[17] Odgaard, M., Klein, K.V., Thysen, S.M., Jimenez-Solem, E., Sillesen, M., Nielsen, M.: CORE-BEHT: A Carefully Optimized and Rigorously Evaluated BEHRT. arXiv. arXiv:2404.15201 [cs] (2024). <https://doi.org/10.48550/arXiv.2404.15201> . <http://arxiv.org/abs/2404.15201> Accessed 2024-12-16

[18] Pang, C., Jiang, X., Kalluri, K.S., Spotnitz, M., Chen, R., Perotte, A., Natarajan, K.: CEHR-BERT: Incorporating temporal information from structured EHR data to improve prediction tasks. arXiv. arXiv:2111.08585 [cs] (2021). <https://doi.org/10.48550/arXiv.2111.08585> . <http://arxiv.org/abs/2111.08585> Accessed 2024-12-16

[19] Li, Y., Rao, S., Solares, J.R.A., Hassaine, A., Ramakrishnan, R., Canoy, D., Zhu, Y., Rahimi, K., Salimi-Khorshidi, G.: BEHRT: Transformer for Electronic Health Records. *Scientific Reports* **10**(1), 7155 (2020) <https://doi.org/10.1038/s41598-020-62922-y> . Publisher: Nature Publishing Group. Accessed 2024-12-16

[20] Waxler, S., Blazek, P., White, D., Sneider, D., Chung, K., Nagarathnam, M., Williams, P., Voeller, H., Wong, K., Swanhorst, M., Zhang, S., Usuyama, N., Wong, C., Naumann, T., Poon, H., Loza, A., Meeker, D., Hain, S., Shah, R.: Generative Medical Event Models Improve with Scale. arXiv. arXiv:2508.12104 [cs] version: 1 (2025). <https://doi.org/10.48550/arXiv.2508.12104> . <http://arxiv.org/abs/2508.12104> Accessed 2025-09-16

[21] Shmatko, A., Jung, A.W., Gaurav, K., Brunak, S., Mortensen, L.H., Birney, E., Fitzgerald, T., Gerstung, M.: Learning the natural history of human disease with generative transformers. *Nature*, 1–9 (2025) <https://doi.org/10.1038/s41586-025-09529-3> . Publisher: Nature Publishing Group. Accessed 2025-10-04

[22] Penedo, G., Malartic, Q., Hesslow, D., Cojocaru, R., Alobeidli, H., Cappelli, A., Pannier, B., Almazrouei, E., Launay, J.: The RefinedWeb Dataset for Falcon LLM: Outperforming Curated Corpora with Web Data Only. *Advances in Neural Information Processing Systems* **36**, 79155–79172 (2023). Accessed 2025-05-01

- [23] Raffel, C., Shazeer, N., Roberts, A., Lee, K., Narang, S., Matena, M., Zhou, Y., Li, W., Liu, P.J.: Exploring the limits of transfer learning with a unified text-to-text transformer. *J. Mach. Learn. Res.* **21**(1), 140–54851405551 (2020)
- [24] Agrawal, M., Heggemann, S., Lang, H., Kim, Y., Sontag, D.: Large Language Models are Few-Shot Clinical Information Extractors. *Proceedings of the 2022 Conference on Empirical Methods in Natural Language Processing, 1998–2022 (2022)* <https://doi.org/10.18653/v1/2022.emnlp-main.130> . Accessed 2024-04-12
- [25] Van Veen, D., Van Uden, C., Blankemeier, L., Delbrouck, J.-B., Aali, A., Bluethgen, C., Pareek, A., Polacin, M., Reis, E.P., Seehofnerová, A., Rohatgi, N., Hosamani, P., Collins, W., Ahuja, N., Langlotz, C.P., Hom, J., Gatidis, S., Pauly, J., Chaudhari, A.S.: Adapted large language models can outperform medical experts in clinical text summarization. *Nature Medicine*, 1–9 (2024) <https://doi.org/10.1038/s41591-024-02855-5> . Publisher: Nature Publishing Group. Accessed 2024-04-11
- [26] Heggemann, S., Buendia, A., Lang, H., Agrawal, M., Jiang, X., Sontag, D.: TabLLM: Few-shot Classification of Tabular Data with Large Language Models. *Proceedings of The 26th International Conference on Artificial Intelligence and Statistics*, 5549–5581 (2023). Accessed 2024-04-12
- [27] Shoham, O.B., Rappoport, N.: CPLLM: Clinical prediction with large language models. *PLOS Digital Health* **3**(12), 0000680 (2024) <https://doi.org/10.1371/journal.pdig.0000680> . Publisher: Public Library of Science. Accessed 2025-09-22
- [28] Zhu, Y., Wang, Z., Gao, J., Tong, Y., An, J., Liao, W., Harrison, E.M., Ma, L., Pan, C.: Prompting Large Language Models for Zero-Shot Clinical Prediction with Structured Longitudinal Electronic Health Record Data. *arXiv. arXiv:2402.01713 [cs]* (2024). <https://doi.org/10.48550/arXiv.2402.01713> . <http://arxiv.org/abs/2402.01713> Accessed 2025-09-22
- [29] Cui, H., Shen, Z., Zhang, J., Shao, H., Qin, L., Ho, J.C., Yang, C.: LLMs-based Few-Shot Disease Predictions using EHR: A Novel Approach Combining Predictive Agent Reasoning and Critical Agent Instruction. *arXiv. arXiv:2403.15464 [cs]* (2024). <https://doi.org/10.48550/arXiv.2403.15464> . <http://arxiv.org/abs/2403.15464> Accessed 2024-12-16
- [30] Acharya, A., Shrestha, S., Chen, A., Conte, J., Avramovic, S., Sikdar, S., Anastasopoulos, A., Das, S.: Clinical risk prediction using language models: benefits and considerations. *Journal of the American Medical Informatics Association* **31**(9), 1856–1864 (2024) <https://doi.org/10.1093/jamia/ocae030> . Accessed 2025-09-22
- [31] Chen, C., Yu, J., Chen, S., Liu, C., Wan, Z., Bitterman, D., Wang, F., Shu, K.: ClinicalBench: Can LLMs Beat Traditional ML Models in Clinical Prediction? *arXiv. arXiv:2411.06469 [cs]* (2024). <https://doi.org/10.48550/arXiv.2411.06469> . <http://arxiv.org/abs/2411.06469> Accessed 2025-09-22

[32] Makarov, N., Bordukova, M., Quengdaeng, P., Garger, D., Rodriguez-Esteban, R., Schmich, F., Menden, M.P.: Large language models forecast patient health trajectories enabling digital twins. *npj Digital Medicine* **8**(1), 588 (2025) <https://doi.org/10.1038/s41746-025-02004-3> . Publisher: Nature Publishing Group. Accessed 2025-10-09

[33] Gao, Y., Myers, S., Chen, S., Dligach, D., Miller, T.A., Bitterman, D., Churpek, M., Afshar, M.: When Raw Data Prevails: Are Large Language Model Embeddings Effective in Numerical Data Representation for Medical Machine Learning Applications? In: Al-Onaizan, Y., Bansal, M., Chen, Y.-N. (eds.) Findings of the Association for Computational Linguistics: EMNLP 2024, pp. 5414–5428. Association for Computational Linguistics, Miami, Florida, USA (2024). <https://doi.org/10.18653/v1/2024.findings-emnlp.311> . <https://aclanthology.org/2024.findings-emnlp.311/> Accessed 2025-09-22

[34] Lee, S.A., Jain, S., Chen, A., Ono, K., Biswas, A., Rudas, A., Fang, J., Chi-ang, J.N.: Clinical decision support using pseudo-notes from multiple streams of EHR data. *npj Digital Medicine* **8**(1), 394 (2025) <https://doi.org/10.1038/s41746-025-01777-x> . Publisher: Nature Publishing Group. Accessed 2025-09-16

[35] Contreras, M., Kapoor, S., Zhang, J., Davidson, A., Ren, Y., Guan, Z., Ozrazgat-Baslanti, T., Nerella, S., Bihorac, A., Rashidi, P.: DeLLiriuM: A large language model for delirium prediction in the ICU using structured EHR. *arXiv. arXiv:2410.17363 [cs]* (2024). <https://doi.org/10.48550/arXiv.2410.17363> . <http://arxiv.org/abs/2410.17363> Accessed 2025-09-22

[36] Brown, T., Mann, B., Ryder, N., Subbiah, M., Kaplan, J.D., Dhariwal, P., Neelakantan, A., Shyam, P., Sastry, G., Askell, A., Agarwal, S., Herbert-Voss, A., Krueger, G., Henighan, T., Child, R., Ramesh, A., Ziegler, D., Wu, J., Winter, C., Hesse, C., Chen, M., Sigler, E., Litwin, M., Gray, S., Chess, B., Clark, J., Berner, C., McCandlish, S., Radford, A., Sutskever, I., Amodei, D.: Language Models are Few-Shot Learners. *Advances in Neural Information Processing Systems* **33**, 1877–1901 (2020). Accessed 2024-05-22

[37] Yang, A., Yang, B., Hui, B., Zheng, B., Yu, B., Zhou, C., Li, C., Li, C., Liu, D., Huang, F., Dong, G., Wei, H., Lin, H., Tang, J., Wang, J., Yang, J., Tu, J., Zhang, J., Ma, J., Yang, J., Xu, J., Zhou, J., Bai, J., He, J., Lin, J., Dang, K., Lu, K., Chen, K., Yang, K., Li, M., Xue, M., Ni, N., Zhang, P., Wang, P., Peng, R., Men, R., Gao, R., Lin, R., Wang, S., Bai, S., Tan, S., Zhu, T., Li, T., Liu, T., Ge, W., Deng, X., Zhou, X., Ren, X., Zhang, X., Wei, X., Ren, X., Liu, X., Fan, Y., Yao, Y., Zhang, Y., Wan, Y., Chu, Y., Liu, Y., Cui, Z., Zhang, Z., Guo, Z., Fan, Z.: Qwen2 Technical Report. *arXiv. arXiv:2407.10671 [cs]* (2024). <https://doi.org/10.48550/arXiv.2407.10671> . <http://arxiv.org/abs/2407.10671> Accessed 2025-01-08

[38] Yang, A., Li, A., Yang, B., Zhang, B., Hui, B., Zheng, B., Yu, B., Gao, C., Huang, C., Lv, C., Zheng, C., Liu, D., Zhou, F., Huang, F., Hu, F., Ge, H., Wei, H., Lin,

H., Tang, J., Yang, J., Tu, J., Zhang, J., Yang, J., Yang, J., Zhou, J., Zhou, J., Lin, J., Dang, K., Bao, K., Yang, K., Yu, L., Deng, L., Li, M., Xue, M., Li, M., Zhang, P., Wang, P., Zhu, Q., Men, R., Gao, R., Liu, S., Luo, S., Li, T., Tang, T., Yin, W., Ren, X., Wang, X., Zhang, X., Ren, X., Fan, Y., Su, Y., Zhang, Y., Zhang, Y., Wan, Y., Liu, Y., Wang, Z., Cui, Z., Zhang, Z., Zhou, Z., Qiu, Z.: Qwen3 Technical Report. arXiv. arXiv:2505.09388 [cs] (2025). <https://doi.org/10.48550/arXiv.2505.09388> . <http://arxiv.org/abs/2505.09388> Accessed 2025-10-04

[39] BehnamGhader, P., Adlakha, V., Mosbach, M., Bahdanau, D., Chapados, N., Reddy, S.: LLM2Vec: Large Language Models Are Secretly Powerful Text Encoders. (2024). <https://openreview.net/forum?id=IW1PR7vEBf> Accessed 2025-03-09

[40] Lee, C., Roy, R., Xu, M., Raiman, J., Shoeybi, M., Catanzaro, B., Ping, W.: NV-Embed: Improved Techniques for Training LLMs as Generalist Embedding Models. arXiv. arXiv:2405.17428 [cs] (2024). <http://arxiv.org/abs/2405.17428> Accessed 2024-08-02

[41] Muennighoff, N., Su, H., Wang, L., Yang, N., Wei, F., Yu, T., Singh, A., Kiela, D.: Generative Representational Instruction Tuning. arXiv. arXiv:2402.09906 [cs] (2024). <http://arxiv.org/abs/2402.09906> Accessed 2024-08-01

[42] Li, Z., Zhang, X., Zhang, Y., Long, D., Xie, P., Zhang, M.: Towards General Text Embeddings with Multi-stage Contrastive Learning. arXiv. arXiv:2308.03281 [cs] (2023). <https://doi.org/10.48550/arXiv.2308.03281> . <http://arxiv.org/abs/2308.03281> Accessed 2024-08-02

[43] Zhang, Y., Li, M., Long, D., Zhang, X., Lin, H., Yang, B., Xie, P., Yang, A., Liu, D., Lin, J., Huang, F., Zhou, J.: Qwen3 Embedding: Advancing Text Embedding and Reranking Through Foundation Models. arXiv. arXiv:2506.05176 [cs] (2025). <https://doi.org/10.48550/arXiv.2506.05176> . <http://arxiv.org/abs/2506.05176> Accessed 2025-09-28

[44] Wornow, M., Thapa, R., Steinberg, E., Fries, J.A., Shah, N.: EHRSHOT: An EHR Benchmark for Few-Shot Evaluation of Foundation Models. (2023). <https://openreview.net/forum?id=CsXC6lcdwl> Accessed 2024-06-12

[45] Steinfeldt, J., Wild, B., Buergel, T., Pietzner, M., Belzen, J., Vauvelle, A., Hegselmann, S., Denaxas, S., Hemingway, H., Langenberg, C., Landmesser, U., Deanfield, J., Eils, R.: Medical history predicts phenome-wide disease onset and enables the rapid response to emerging health threats. *Nature Communications* **16**(1), 585 (2025) <https://doi.org/10.1038/s41467-025-55879-x> . Publisher: Nature Publishing Group. Accessed 2025-02-15

[46] Sudlow, C., Gallacher, J., Allen, N., Beral, V., Burton, P., Danesh, J., Downey, P., Elliott, P., Green, J., Landray, M., Liu, B., Matthews, P., Ong, G., Pell, J., Silman, A., Young, A., Sprosen, T., Peakman, T., Collins, R.: UK Biobank: An

Open Access Resource for Identifying the Causes of a Wide Range of Complex Diseases of Middle and Old Age. PLOS Medicine **12**(3), 1001779 (2015) <https://doi.org/10.1371/journal.pmed.1001779> . Publisher: Public Library of Science. Accessed 2025-05-01

[47] Bycroft, C., Freeman, C., Petkova, D., Band, G., Elliott, L.T., Sharp, K., Motyer, A., Vukcevic, D., Delaneau, O., O'Connell, J., Cortes, A., Welsh, S., Young, A., Effingham, M., McVean, G., Leslie, S., Allen, N., Donnelly, P., Marchini, J.: The UK Biobank resource with deep phenotyping and genomic data. Nature **562**(7726), 203–209 (2018) <https://doi.org/10.1038/s41586-018-0579-z> . Number: 7726 Publisher: Nature Publishing Group. Accessed 2022-11-21

[48] Grattafiori, A., Dubey, A., Jauhri, A., Pandey, A., Kadian, A., Al-Dahle, A., Letman, A., Mathur, A., Schelten, A., Vaughan, A., Yang, A., Fan, A., Goyal, A., Hartshorn, A., Yang, A., Mitra, A., Sravankumar, A., Korenev, A., Hinsvark, A., Rao, A., Zhang, A., Rodriguez, A., Gregerson, A., Spataru, A., Roziere, B., Biron, B., Tang, B., Chern, B., Caucheteux, C., Nayak, C., Bi, C., Marra, C., McConnell, C., Keller, C., Touret, C., Wu, C., Wong, C., Ferrer, C.C., Nikolaidis, C., Allonsius, D., Song, D., Pintz, D., Livshits, D., Wyatt, D., Esiobu, D., Choudhary, D., Mahajan, D., Garcia-Olano, D., Perino, D., Hupkes, D., Lakomkin, E., AlBadawy, E., Lobanova, E., Dinan, E., Smith, E.M., Radenovic, F., Guzmán, F., Zhang, F., Synnaeve, G., Lee, G., Anderson, G.L., Thattai, G., Nail, G., Mialon, G., Pang, G., Cucurell, G., Nguyen, H., Korevaar, H., Xu, H., Touvron, H., Zarov, I., Ibarra, I.A., Kloumann, I., Misra, I., Evtimov, I., Zhang, J., Copet, J., Lee, J., Geffert, J., Vranes, J., Park, J., Mahadeokar, J., Shah, J., Linde, J.v.d., Billock, J., Hong, J., Lee, J., Fu, J., Chi, J., Huang, J., Liu, J., Wang, J., Yu, J., Bitton, J., Spisak, J., Park, J., Rocca, J., Johnstun, J., Saxe, J., Jia, J., Alwala, K.V., Prasad, K., Upasani, K., Plawiak, K., Li, K., Heafield, K., Stone, K., El-Arini, K., Iyer, K., Malik, K., Chiu, K., Bhalla, K., Lakhota, K., Rantala-Yeary, L., Maaten, L.v.d., Chen, L., Tan, L., Jenkins, L., Martin, L., Madaan, L., Malo, L., Blecher, L., Landzaat, L., Oliveira, L.d., Muzzi, M., Pasupuleti, M., Singh, M., Paluri, M., Kardas, M., Tsimpoukelli, M., Oldham, M., Rita, M., Pavlova, M., Kambadur, M., Lewis, M., Si, M., Singh, M.K., Hassan, M., Goyal, N., Torabi, N., Bashlykov, N., Bogoychev, N., Chatterji, N., Zhang, N., Duchenne, O., Çelebi, O., Alrassy, P., Zhang, P., Li, P., Vasic, P., Weng, P., Bhargava, P., Dubal, P., Krishnan, P., Koura, P.S., Xu, P., He, Q., Dong, Q., Srinivasan, R., Ganapathy, R., Calderer, R., Cabral, R.S., Stojnic, R., Raileanu, R., Maheswari, R., Girdhar, R., Patel, R., Sauvestre, R., Polidoro, R., Sumbaly, R., Taylor, R., Silva, R., Hou, R., Wang, R., Hosseini, S., Chennabasappa, S., Singh, S., Bell, S., Kim, S.S., Edunov, S., Nie, S., Narang, S., Raparthy, S., Shen, S., Wan, S., Bhosale, S., Zhang, S., Vandenhende, S., Batra, S., Whitman, S., Sootla, S., Collot, S., Gururangan, S., Borodinsky, S., Herman, T., Fowler, T., Sheasha, T., Georgiou, T., Scialom, T., Speckbacher, T., Mihaylov, T., Xiao, T., Karn, U., Goswami, V., Gupta, V., Ramanathan, V., Kerkez, V., Gonguet, V., Do, V., Vogeti, V., Albiero, V., Petrovic, V., Chu, W., Xiong, W., Fu, W., Meers, W., Martinet, X., Wang, X., Wang, X., Tan, X.E., Xia, X., Xie, X., Jia, X., Wang, X., Goldschlag,

Y., Gaur, Y., Babaei, Y., Wen, Y., Song, Y., Zhang, Y., Li, Y., Mao, Y., Coudert, Z.D., Yan, Z., Chen, Z., Papakipos, Z., Singh, A., Srivastava, A., Jain, A., Kelsey, A., Shajnfeld, A., Gangidi, A., Victoria, A., Goldstand, A., Menon, A., Sharma, A., Boesenberg, A., Baevski, A., Feinstein, A., Kallet, A., Sangani, A., Teo, A., Yunus, A., Lupu, A., Alvarado, A., Caples, A., Gu, A., Ho, A., Poulton, A., Ryan, A., Ramchandani, A., Dong, A., Franco, A., Goyal, A., Saraf, A., Chowdhury, A., Gabriel, A., Bharambe, A., Eisenman, A., Yazdan, A., James, B., Maurer, B., Leonhardi, B., Huang, B., Loyd, B., Paola, B.D., Paranjape, B., Liu, B., Wu, B., Ni, B., Hancock, B., Wasti, B., Spence, B., Stojkovic, B., Gamido, B., Montalvo, B., Parker, C., Burton, C., Mejia, C., Liu, C., Wang, C., Kim, C., Zhou, C., Hu, C., Chu, C.-H., Cai, C., Tindal, C., Feichtenhofer, C., Gao, C., Civin, D., Beaty, D., Kreymer, D., Li, D., Adkins, D., Xu, D., Testuggine, D., David, D., Parikh, D., Liskovich, D., Foss, D., Wang, D., Le, D., Holland, D., Dowling, E., Jamil, E., Montgomery, E., Presani, E., Hahn, E., Wood, E., Le, E.-T., Brinkman, E., Arcaute, E., Dunbar, E., Smothers, E., Sun, F., Kreuk, F., Tian, F., Kokkinos, F., Ozgenel, F., Caggioni, F., Kanayet, F., Seide, F., Florez, G.M., Schwarz, G., Badeer, G., Swee, G., Halpern, G., Herman, G., Sizov, G., Guangyi, Zhang, Lakshminarayanan, G., Inan, H., Shojanazeri, H., Zou, H., Wang, H., Zha, H., Habeeb, H., Rudolph, H., Suk, H., Aspegren, H., Goldman, H., Zhan, H., Damlaj, I., Molybog, I., Tufanov, I., Leontiadis, I., Veliche, I.-E., Gat, I., Weissman, J., Geboski, J., Kohli, J., Lam, J., Asher, J., Gaya, J.-B., Marcus, J., Tang, J., Chan, J., Zhen, J., Reizenstein, J., Teboul, J., Zhong, J., Jin, J., Yang, J., Cummings, J., Carvill, J., Shepard, J., McPhie, J., Torres, J., Ginsburg, J., Wang, J., Wu, K., U, K.H., Saxena, K., Khandelwal, K., Zand, K., Matosich, K., Veeraraghavan, K., Michelena, K., Li, K., Jagadeesh, K., Huang, K., Chawla, K., Huang, K., Chen, L., Garg, L., A, L., Silva, L., Bell, L., Zhang, L., Guo, L., Yu, L., Moshkovich, L., Wehrstedt, L., Khabsa, M., Avalani, M., Bhatt, M., Mankus, M., Hasson, M., Lennie, M., Reso, M., Groshev, M., Naumov, M., Lathi, M., Keneally, M., Liu, M., Seltzer, M.L., Valko, M., Restrepo, M., Patel, M., Vyatskov, M., Samvelyan, M., Clark, M., Macey, M., Wang, M., Hermoso, M.J., Metanat, M., Rastegari, M., Bansal, M., Santhanam, N., Parks, N., White, N., Bawa, N., Singhal, N., Egebo, N., Usunier, N., Mehta, N., Laptev, N.P., Dong, N., Cheng, N., Chernoguz, O., Hart, O., Salpekar, O., Kalinli, O., Kent, P., Parekh, P., Saab, P., Balaji, P., Rittner, P., Bontrager, P., Roux, P., Dollar, P., Zvyagina, P., Ratanchandani, P., Yuvraj, P., Liang, Q., Alao, R., Rodriguez, R., Ayub, R., Murthy, R., Nayani, R., Mitra, R., Parthasarathy, R., Li, R., Hogan, R., Battey, R., Wang, R., Howes, R., Rinott, R., Mehta, S., Siby, S., Bondu, S.J., Datta, S., Chugh, S., Hunt, S., Dhillon, S., Sidorov, S., Pan, S., Mahajan, S., Verma, S., Yamamoto, S., Ramaswamy, S., Lindsay, S., Lindsay, S., Feng, S., Lin, S., Zha, S.C., Patil, S., Shankar, S., Zhang, S., Zhang, S., Wang, S., Agarwal, S., Sajuyigbe, S., Chintala, S., Max, S., Chen, S., Kehoe, S., Satterfield, S., Govindaprasad, S., Gupta, S., Deng, S., Cho, S., Virk, S., Subramanian, S., Choudhury, S., Goldman, S., Remez, T., Glaser, T., Best, T., Koehler, T., Robinson, T., Li, T., Zhang, T., Matthews, T., Chou, T., Shaked, T., Vontimitta, V.,

Ajaii, V., Montanez, V., Mohan, V., Kumar, V.S., Mangla, V., Ionescu, V., Poenaru, V., Mihailescu, V.T., Ivanov, V., Li, W., Wang, W., Jiang, W., Bouaziz, W., Constable, W., Tang, X., Wu, X., Wang, X., Wu, X., Gao, X., Kleinman, Y., Chen, Y., Hu, Y., Jia, Y., Qi, Y., Li, Y., Zhang, Y., Zhang, Y., Adi, Y., Nam, Y., Yu, Wang, Zhao, Y., Hao, Y., Qian, Y., Li, Y., He, Y., Rait, Z., DeVito, Z., Rosnbrick, Z., Wen, Z., Yang, Z., Zhao, Z., Ma, Z.: The Llama 3 Herd of Models. arXiv. arXiv:2407.21783 [cs] (2024). <https://doi.org/10.48550/arXiv.2407.21783> . <http://arxiv.org/abs/2407.21783> Accessed 2025-01-08

[49] Jiang, L.Y., Liu, X.C., Nejatian, N.P., Nasir-Moin, M., Wang, D., Abidin, A., Eaton, K., Riina, H.A., Laufer, I., Punjabi, P., Miceli, M., Kim, N.C., Orillac, C., Schnurman, Z., Livia, C., Weiss, H., Kurland, D., Neifert, S., Dastagirzada, Y., Kondziolka, D., Cheung, A.T.M., Yang, G., Cao, M., Flores, M., Costa, A.B., Aphinyanaphongs, Y., Cho, K., Oermann, E.K.: Health system-scale language models are all-purpose prediction engines. *Nature* **619**(7969), 357–362 (2023) <https://doi.org/10.1038/s41586-023-06160-y> . Publisher: Nature Publishing Group. Accessed 2024-07-31

[50] Lehne, M., Sass, J., Essenwanger, A., Schepers, J., Thun, S.: Why digital medicine depends on interoperability. *npj Digital Medicine* **2**(1), 1–5 (2019) <https://doi.org/10.1038/s41746-019-0158-1> . Publisher: Nature Publishing Group. Accessed 2025-02-15

[51] Kirchler, M., Ferro, M., Lorenzini, V., FinnGen, Lippert, C., Ganna, A.: Large language models improve transferability of electronic health record-based predictions across countries and coding systems. *medRxiv*. Pages: 2025.02.03.25321597 (2025). <https://doi.org/10.1101/2025.02.03.25321597> . <https://www.medrxiv.org/content/10.1101/2025.02.03.25321597v1> Accessed 2025-02-15

[52] Moor, M., Banerjee, O., Abad, Z.S.H., Krumholz, H.M., Leskovec, J., Topol, E.J., Rajpurkar, P.: Foundation models for generalist medical artificial intelligence. *Nature* **616**(7956), 259–265 (2023) <https://doi.org/10.1038/s41586-023-05881-4> . Publisher: Nature Publishing Group. Accessed 2025-02-15

[53] Ke, G., Meng, Q., Finley, T., Wang, T., Chen, W., Ma, W., Ye, Q., Liu, T.-Y.: LightGBM: A Highly Efficient Gradient Boosting Decision Tree. *Advances in Neural Information Processing Systems* **30** (2017). Accessed 2022-08-01

[54] Liu, Q., Chen, B., Guo, J., Ziyadi, M., Lin, Z., Chen, W., Lou, J.-G.: TAPEX: Table Pre-training via Learning a Neural SQL Executor. (2021). <https://openreview.net/forum?id=O50443AsCP> Accessed 2025-01-18

[55] Li, P., He, Y., Yashar, D., Cui, W., Ge, S., Zhang, H., Rifinski Fainman, D., Zhang, D., Chaudhuri, S.: Table-GPT: Table Fine-tuned GPT for Diverse Table Tasks. *Proceedings of the ACM on Management of Data* **2**(3), 1–28 (2024) <https://doi.org/10.1145/3654979> . Accessed 2025-01-18

[56] Dong, H., Zhao, J., Tian, Y., Xiong, J., Zhou, M., Lin, Y., Cambronero, J., He, Y., Han, S., Zhang, D.: Encoding Spreadsheets for Large Language Models. In: Al-Onaizan, Y., Bansal, M., Chen, Y.-N. (eds.) Proceedings of the 2024 Conference on Empirical Methods in Natural Language Processing, pp. 20728–20748. Association for Computational Linguistics, Miami, Florida, USA (2024). <https://doi.org/10.18653/v1/2024.emnlp-main.1154> . <https://aclanthology.org/2024.emnlp-main.1154/> Accessed 2025-01-18

[57] Sui, Y., Zhou, M., Zhou, M., Han, S., Zhang, D.: Table Meets LLM: Can Large Language Models Understand Structured Table Data? A Benchmark and Empirical Study. In: Proceedings of the 17th ACM International Conference on Web Search and Data Mining, pp. 645–654. ACM, Merida Mexico (2024). <https://doi.org/10.1145/3616855.3635752> . <https://dl.acm.org/doi/10.1145/3616855.3635752> Accessed 2025-01-18

[58] Springer, J.M., Kotha, S., Fried, D., Neubig, G., Raghunathan, A.: Repetition Improves Language Model Embeddings. arXiv. arXiv:2402.15449 [cs] (2024). <https://doi.org/10.48550/arXiv.2402.15449> . <http://arxiv.org/abs/2402.15449> Accessed 2024-08-01

[59] Wang, A., Liu, C., Yang, J., Weng, C.: Fine-tuning Large Language Models for Rare Disease Concept Normalization. bioRxiv. Pages: 2023.12.28.573586 Section: New Results (2024). <https://doi.org/10.1101/2023.12.28.573586> . <https://www.biorxiv.org/content/10.1101/2023.12.28.573586v3> Accessed 2024-07-26

[60] He, P., Gao, J., Chen, W.: DeBERTaV3: Improving DeBERTa using ELECTRA-Style Pre-Training with Gradient-Disentangled Embedding Sharing. (2022). <https://openreview.net/forum?id=sE7-XhLxHA> Accessed 2025-01-19

[61] Lee, J., Yoon, W., Kim, S., Kim, D., Kim, S., So, C.H., Kang, J.: BioBERT: a pre-trained biomedical language representation model for biomedical text mining. Bioinformatics **36**(4), 1234–1240 (2020) <https://doi.org/10.1093/bioinformatics/btz682> . Accessed 2022-04-26

[62] Alsentzer, E., Murphy, J., Boag, W., Weng, W.-H., Jindi, D., Naumann, T., McDermott, M.: Publicly Available Clinical BERT Embeddings. In: Rumshisky, A., Roberts, K., Bethard, S., Naumann, T. (eds.) Proceedings of the 2nd Clinical Natural Language Processing Workshop, pp. 72–78. Association for Computational Linguistics, Minneapolis, Minnesota, USA (2019). <https://doi.org/10.18653/v1/W19-1909> . <https://aclanthology.org/W19-1909/> Accessed 2025-01-19

[63] VasanthaRajan, C., Tun, K.Z., Thi-Nga, H., Jain, S., Rong, T., Siong, C.E.: MedBERT: A Pre-trained Language Model for Biomedical Named Entity Recognition. In: 2022 Asia-Pacific Signal and Information Processing Association Annual Summit and Conference (APSIPA ASC), pp. 1482–1488. IEEE, Chiang Mai, Thailand (2022). <https://doi.org/10.23919/APSIPAASC55919.2022.9980157> . <https://ieeexplore.ieee.org/document/9980157/> Accessed 2025-10-05

[64] Hu, E.J., Shen, Y., Wallis, P., Allen-Zhu, Z., Li, Y., Wang, S., Wang, L., Chen, W.: LoRA: Low-Rank Adaptation of Large Language Models. arXiv preprint arXiv:2106.09685 (2021). Accessed 2023-11-10

[65] Ma, M.D., Wang, X., Xiao, Y., Cuturrufo, A., Nori, V.S., Halperin, E., Wang, W.: Memorize and Rank: Elevating Large Language Models for Clinical Diagnosis Prediction. Proceedings of the AAAI Conference on Artificial Intelligence **39**(23), 24786–24794 (2025) <https://doi.org/10.1609/aaai.v39i23.34660> . Accessed 2025-09-22

[66] Wu, P., Gifford, A., Meng, X., Li, X., Campbell, H., Varley, T., Zhao, J., Carroll, R., Bastarache, L., Denny, J.C., Theodoratou, E., Wei, W.-Q.: Mapping ICD-10 and ICD-10-CM Codes to Phecodes: Workflow Development and Initial Evaluation. JMIR Medical Informatics **7**(4), 14325 (2019) <https://doi.org/10.2196/14325> . Company: JMIR Medical Informatics Distributor: JMIR Medical Informatics Institution: JMIR Medical Informatics Label: JMIR Medical Informatics Publisher: JMIR Publications Inc., Toronto, Canada. Accessed 2025-05-01

[67] Wei, W.-Q., Bastarache, L.A., Carroll, R.J., Marlo, J.E., Osterman, T.J., Gamanon, E.R., Cox, N.J., Roden, D.M., Denny, J.C.: Evaluating phecodes, clinical classification software, and ICD-9-CM codes for genome-wide association studies in the electronic health record. PLOS ONE **12**(7), 0175508 (2017) <https://doi.org/10.1371/journal.pone.0175508> . Publisher: Public Library of Science. Accessed 2025-05-01

[68] Denaxas, S., Shah, A.D., Mateen, B.A., Kuan, V., Quint, J.K., Fitzpatrick, N., Torralbo, A., Fatemifar, G., Hemingway, H.: A semi-supervised approach for rapidly creating clinical biomarker phenotypes in the UK Biobank using different primary care EHR and clinical terminology systems. JAMIA Open **3**(4), 545–556 (2020) <https://doi.org/10.1093/jamiaopen/ooaa047> . Accessed 2025-05-01

[69] Arnrich, B., Choi, E., Fries, J.A., McDermott, M.B.A., Oh, J., Pollard, T.J., Shah, N., Steinberg, E., Wornow, M., Water, R.: Medical Event Data Standard (MEDS): Facilitating Machine Learning for Health. In: ICLR 2024 Workshop on Learning from Time Series For Health (2024). <https://openreview.net/forum?id=lsHy2ebjIG>

A Appendix

A.1 Additional Experimental Details

Table 7 UK Biobank Prediction Tasks Overview. Overview of clinical prediction tasks of UKB spanning three different task groups. Total Labels refers to the number of patients after filtering out patients with records prior to prediction. The prediction window for all tasks is 1 year (similar to *Assignment of New Diagnoses* Task as in [44]).

Attribute	Total Labels (Positive)
Mortality prediction	
Mortality (Death)	359245 (802)
Operational Outcomes	
Hospitalization	359250 (68505)
Assignment of New Diagnoses	
Cardiac arrest	358963 (87)
Abdominal aortic aneurysm	358926 (73)
Parkinson's disease (Primary)	358729 (86)
Aortic stenosis	358384 (114)
Rheumatic fever and chronic rheumatic heart diseases	358064 (154)
Mitral valve insufficiency	357949 (186)
Endocarditis	357876 (79)
Suicide ideation and attempt or self harm	357652 (175)
Cerebral infarction [Ischemic stroke]	357180 (310)
Pulmonary embolism	357158 (248)
Atrial fibrillation	357154 (306)
Heart failure	356657 (435)
Rheumatoid arthritis	356029 (316)
Chronic obstructive pulmonary disease [COPD]	354513 (923)
Psoriasis	353400 (410)
Chronic kidney disease	353396 (1001)
Pneumonia	353232 (802)
Myocardial infarction [Heart attack]	351970 (619)
Diabetes mellitus	344185 (1841)
Ischemic heart disease	341574 (1788)
Anemia	343235 (1814)
Back pain	300529 (3933)
Hypertension	300334 (7653)

Table 8 Semantic Codes for Aggregated Concepts in EHR Serialization. We aggregated time-series data encoded via LOINC concepts and identified the most frequent concepts from which we selected 24 key medical concepts. To reduce duplicate information, we merged synonymous semantic codes. The primary LOINC codes are presented first in the column Semantic Codes followed by identified duplicates. We also defined a unit, minimum and maximum allowed values for filtering, a normal range to classify values in low, normal, and high, and a formatting strategy to create our EHR serialization.

Medical Concept	Semantic Codes	Unit	Min-Max Range	Normal Range	Formatting
Recent Body Metrics					
Body weight	LOINC/29463-7	oz	350-10000		One decimal
Body height	LOINC/8302-2	inch	5-100		One decimal
Body mass index / BMI	LOINC/39156-5	kg/m ²	10-100	18.5-24.9	One decimal
Body surface area	LOINC/8277-6, SNOMED/301898006	m ²	0.1-10		Two decimals
Recent Vital Signs					
Heart rate	LOINC/8867-4, SNOMED/364075005, SNOMED/78564009	bpm	5-300	60-100	Integer
Systolic blood pressure	LOINC/8480-6, SNOMED/271649006	mmHg	20-300	90-140	Integer
Diastolic blood pressure	LOINC/8462-4, SNOMED/271650006	mmHg	20-300	60-90	Integer
Body temperature	LOINC/8310-5	°F	80-120	95-100.4	One decimal
Respiratory rate	LOINC/9279-1	breaths/min	1-100	12-18	Integer
Oxygen saturation	LOINC/LP21258-6	%	1-100	95-100	Integer
Recent Lab Results					
Hemoglobin	LOINC/718-7, SNOMED/271026005, SNOMED/441689006	g/dL	1-20	12-17	One decimal
Hematocrit	LOINC/4544-3, LOINC/20570-8, LOINC/48703-3, SNOMED/28317006	%	10-100	36-51	Integer
Erythrocytes	LOINC/789-8, LOINC/26453-1	106/uL	1-10	4.2-5.9	Two decimals
Leukocytes	LOINC/20584-9, LOINC/6690-2	103/uL	1-100	4-10	One decimal
Platelets	LOINC/777-3, SNOMED/61928009	103/uL	10-1000	150-350	Integer
Sodium	LOINC/2951-2, LOINC/2947-0, SNOMED/25197003	mmol/L	100-200	136-145	Integer
Potassium	LOINC/2823-3, SNOMED/312468003, LOINC/6298-4, SNOMED/59573005	mmol/L	0.1-10	3.5-5.0	One decimal
Chloride	LOINC/2075-0, SNOMED/104589004, LOINC/2069-3	mmol/L	50-200	98-106	Integer
Carbon dioxide, total	LOINC/2028-9	mmol/L	10-100	23-28	Integer
Calcium	LOINC/17861-6, SNOMED/271240001	mg/dL	1-20	9-10.5	One decimal
Glucose	LOINC/2345-7, SNOMED/166900001, LOINC/2339-0, SNOMED/33747003, LOINC/14749-6	mg/dL	10-1000	70-100	Integer
Urea nitrogen	LOINC/3094-0, SNOMED/105011006	mg/dL	1-200	8-20	Integer
Creatinine	LOINC/2160-0, SNOMED/113075003	mg/dL	0.1-10	0.7-1.3	One decimal
Anion gap	LOINC/33037-3, LOINC/41276-7, SNOMED/25469001	mmol/L	-20-50	3-11	Integer

Table 9 Instructions for LLM Embedding Models. The LLM embedding models were trained using instructions; hence, we also defined simple task-specific prompts for each of the 15 clinical prediction tasks. Each prompt is prepended by the prefix given below, containing a general task description. The three tasks used for the external validation on UKB use a similar design. For the decoder model we added an additional instruction to the prompt enforcing the output of Yes and No tokens used for prediction.

Task	Prompt
Prefix (for all tasks)	Given a patient's electronic healthcare record (EHR) in Markdown format, retrieve relevant passages that answer the query:
EHRSHOT	
Long Length of Stay	will the patient stay in the hospital for more than 7 days
30-day Readmission	will the patient be readmitted to the hospital within 30 days
ICU Transfer	will the patient be transferred to the intensive care unit
Thrombocytopenia	has the patient thrombocytopenia
Hyperkalemia	has the patient hyperkalemia
Hypoglycemia	has the patient hypoglycemia
Hyponatremia	has the patient hyponatremia
Anemia	has the patient anemia
Hypertension	has the patient hypertension
Hyperlipidemia	has the patient hyperlipidemia
Pancreatic Cancer	has the patient pancreatic cancer
Celiac	has the patient celiac disease
Lupus	has the patient lupus
Acute MI	has the patient an acute myocardial infarction
Chest X-Ray Findings	what are the chest x-ray findings of the patient
Generic (ablation)	what are the key clinical features of the patient to predict future medical events
UK Biobank (UKB)	
Mortality Prediction	will the patient die in the next 1 year
Hospitalization	will the patient be hospitalized in the next 1 year
Assignment of New Diagnoses	has the patient a medical condition
Additional Prompt Added for Decoder Qwen3-8B	
Decoder Prompt	Answer STRICTLY with a single token: Yes or No. No punctuation, no extra words.

A.2 Full Results on EHRSHOT

Table 10 Performance for All Examples on EHRSHOT. Mean area under the receiver operating characteristic curve (AUROC) performance and bootstrapped 95% confidence intervals of all included models for four task groups. The macro-averaged performance across all task groups is given in the right-most column. All LLM embedding models use a context size of 8,192 tokens.

Model	Operational Outcomes	Anticipating Lab Test Results	Assignment of New Diagnosis	Anticipating Chest X-ray Findings	Macro Avg. Across Task Groups
Baselines [44]					
CLMBR-T-Base	0.824 .803-.845	0.832 .824-.840	0.707 .667-.746	0.713 .702-.724	0.769 .746-.792
Count-based + GBM	0.774 .752-.797	0.728 .716-.741	0.719 .669-.768	0.656 .641-.671	0.719 .691-.748
LLM Embedding Models					
Qwen3-Emb-8B	0.776 .753-.800	0.859 .852-.866	0.717 .669-.765	0.691 .678-.704	0.761 .733-.788
Qwen3-Emb-4B	0.754 .729-.780	0.856 .849-.864	0.654 .612-.696	0.690 .678-.702	0.739 .713-.764
Qwen3-Emb-0.6B	0.749 .723-.775	0.800 .790-.810	0.683 .633-.733	0.656 .643-.669	0.722 .693-.752
Qwen2-Emb-7B	0.775 .752-.797	0.784 .774-.795	0.684 .638-.729	0.678 .666-.691	0.730 .704-.757
Qwen2-Emb-1.5B	0.762 .740-.783	0.739 .727-.750	0.690 .638-.742	0.661 .649-.674	0.713 .683-.742
Llama3.1-LLM2Vec-8B	0.767 .744-.791	0.760 .748-.771	0.708 .655-.762	0.689 .676-.701	0.731 .701-.762
LLM Embedding Model + EHR Foundation Model [44]					
Qwen3-Emb-8B + CLMBR-T-Base	0.812 .791-.833	0.880 .874-.886	0.728 .682-.775	0.717 .705-.728	0.784 .758-.811
LLM Embedding Model + GBM Head					
Qwen3-Emb-8B + GBM	0.742 .718-.765	0.831 .823-.839	0.713 .669-.758	0.669 .657-.682	0.739 .713-.765
Multiple Embedding Model for EHR (MEME) [34] with Linear Head					
Qwen3-Emb-8B MEME	0.786 .763-.810	0.882 .876-.888	0.735 .690-.780	0.680 .667-.692	0.771 .745-.797
MedBERT MEME	0.752 .730-.775	0.840 .832-.849	0.697 .645-.748	0.648 .633-.663	0.734 .705-.764
Encoder Language Models with Chunked Inputs					
ClinicalBERT	0.740 .715-.765	0.736 .725-.748	0.703 .659-.748	0.649 .636-.663	0.707 .680-.734
MedBERT	0.730 .705-.756	0.735 .723-.747	0.661 .603-.718	0.650 .638-.663	0.694 .661-.727
DeBERTaV3 large	0.718 .690-.746	0.703 .691-.716	0.665 .620-.709	0.617 .603-.632	0.676 .648-.704
DeBERTaV3 base	0.715 .687-.743	0.697 .685-.710	0.646 .601-.690	0.622 .608-.635	0.670 .642-.698
BERT large	0.728 .703-.753	0.719 .707-.730	0.666 .619-.714	0.637 .623-.651	0.688 .659-.716
BERT base	0.739 .713-.764	0.719 .707-.730	0.677 .630-.725	0.633 .620-.647	0.692 .664-.720

Table 11 Performance for All Examples on EHRSHOT for Different Serializations.
 Area under the receiver operating characteristic curve (AUROC) performance and bootstrapped 95% confidence intervals of the Markdown EHR serialization, the alternative data formats (JSON, XML, YAML), and four alternative serializations containing all events as newline separated list.

Model	Operational Outcomes	Anticipating Lab Test Results	Assignment of New Diagnosis	Anticipating Chest X-ray Findings	Macro Avg. Across Task Groups
EHR Serialization Formats					
Markdown (ours)	0.776 .753-.800	0.859 .852-.866	0.717 .669-.765	0.691 .678-.704	0.761 .733-.788
List events	0.799 .776-.822	0.756 .745-.767	0.727 .692-.762	0.721 .710-.732	0.751 .728-.773
List events old	0.763 .740-.787	0.710 .696-.723	0.730 .689-.772	0.674 .660-.688	0.719 .694-.745
List events with time	0.798 .776-.820	0.753 .742-.764	0.730 .687-.773	0.724 .712-.735	0.751 .726-.776
List events old with time	0.769 .747-.791	0.700 .686-.713	0.699 .660-.739	0.674 .659-.688	0.710 .686-.735
JSON	0.774 .750-.797	0.857 .850-.864	0.710 .669-.751	0.690 .676-.703	0.758 .733-.783
XML	0.764 .740-.789	0.863 .856-.870	0.712 .670-.755	0.682 .669-.696	0.755 .730-.781
YAML	0.775 .751-.799	0.861 .854-.868	0.722 .675-.768	0.687 .674-.701	0.761 .734-.789

Table 12 Performance for All Examples on EHRSHOT for EHR Serialization

Experiments. Area under the receiver operating characteristic curve (AUROC) performance and bootstrapped 95% confidence intervals of the Markdown EHR serialization used in this work (Full EHR) and different EHR serialization variants. We evaluated a generic and an empty instruction, serializations with specific components removed, and serialization consisting of an individual component.

Model	Operational Outcomes	Anticipating Lab Test Results	Assignment of New Diagnosis	Anticipating Chest X-ray Findings	Macro Avg. Across Task Groups
Original Markdown Serialization with 4,096 Tokens					
Full EHR	0.772 .749-.795	0.866 .859-.873	0.705 .667-.743	0.674 .661-.688	0.754 .731-.778
Instruction Experiments					
Generic Instruction	0.762 .737-.786	0.829 .821-.838	0.689 .653-.726	0.673 .659-.687	0.738 .715-.762
Empty Instruction	0.758 .733-.784	0.796 .787-.805	0.696 .657-.734	0.671 .657-.684	0.730 .705-.755
Removing Serialization Components					
No Demographics	0.764 .741-.787	0.866 .860-.873	0.706 .663-.749	0.678 .666-.691	0.754 .728-.779
No Body Metrics	0.768 .743-.792	0.866 .860-.873	0.713 .675-.752	0.677 .663-.690	0.756 .732-.780
No Vital Signs	0.767 .741-.792	0.866 .859-.873	0.702 .659-.744	0.671 .658-.684	0.751 .725-.777
No Lab Results	0.771 .747-.794	0.719 .706-.731	0.704 .662-.745	0.680 .667-.693	0.718 .692-.744
No Visits	0.763 .739-.787	0.865 .858-.872	0.720 .666-.774	0.681 .668-.695	0.757 .727-.788
No Conditions	0.767 .742-.792	0.868 .860-.875	0.736 .696-.775	0.665 .652-.678	0.759 .734-.783
No Medications	0.761 .738-.785	0.866 .859-.873	0.690 .650-.730	0.675 .661-.688	0.748 .724-.772
No Procedures	0.772 .749-.795	0.868 .861-.874	0.700 .662-.737	0.676 .663-.689	0.754 .730-.777
Individual Serialization Components					
Only Demographics	0.572 .541-.602	0.544 .528-.559	0.609 .577-.641	0.511 .495-.527	0.559 .534-.584
Only Body Metrics	0.694 .670-.718	0.591 .579-.603	0.517 .484-.551	0.564 .552-.577	0.592 .569-.614
Only Vital Signs	0.607 .577-.637	0.622 .609-.634	0.540 .501-.580	0.600 .589-.612	0.592 .566-.618
Only Lab Results	0.678 .650-.706	0.887 .882-.893	0.637 .594-.679	0.607 .594-.619	0.702 .676-.728
Only Visits	0.623 .596-.650	0.652 .639-.665	0.586 .541-.631	0.638 .626-.649	0.625 .597-.652
Only Conditions	0.759 .736-.781	0.714 .701-.727	0.681 .631-.731	0.676 .663-.689	0.707 .679-.736
Only Medications	0.745 .720-.770	0.687 .674-.700	0.690 .644-.736	0.645 .633-.657	0.692 .664-.719
Only Procedures	0.744 .718-.770	0.689 .675-.703	0.680 .641-.719	0.654 .642-.666	0.692 .667-.717

Table 13 Performance for All Examples on EHRSHOT Across Context Sizes. Area under the receiver operating characteristic curve (AUROC) performance and bootstrapped 95% confidence intervals for different context sizes of the LLM embedding models.

Model	Operational Outcomes	Anticipating Lab Test Results	Assignment of New Diagnosis	Anticipating Chest X-ray Findings	Macro Avg. Across Task Groups
Qwen3-Emb-8B					
8,192 context size	0.776 .753-.800	0.859 .852-.866	0.717 .669-.765	0.691 .678-.704	0.761 .733-.788
4,096 context size	0.772 .749-.795	0.866 .859-.873	0.705 .667-.743	0.674 .661-.688	0.754 .731-.778
2,048 context size	0.751 .727-.775	0.876 .870-.882	0.699 .657-.742	0.651 .637-.666	0.744 .719-.770
1,024 context size	0.725 .701-.750	0.879 .873-.885	0.642 .592-.693	0.639 .624-.653	0.721 .692-.750
512 context size	0.703 .678-.728	0.742 .731-.754	0.639 .591-.686	0.618 .603-.633	0.676 .647-.704
Qwen2-Emb-7B					
8,192 context size	0.775 .752-.797	0.784 .774-.795	0.684 .638-.729	0.678 .666-.691	0.730 .704-.757
4,096 context size	0.771 .747-.795	0.865 .858-.873	0.716 .675-.757	0.666 .653-.680	0.755 .730-.780
2,048 context size	0.745 .720-.770	0.877 .871-.883	0.725 .683-.767	0.656 .642-.670	0.751 .725-.776
1,024 context size	0.731 .706-.756	0.885 .879-.891	0.677 .638-.716	0.643 .629-.656	0.734 .710-.758
512 context size	0.690 .664-.716	0.740 .729-.751	0.642 .606-.678	0.612 .597-.628	0.671 .647-.695
Llama3.1-LLM2Vec-8B					
8,192 context size	0.767 .744-.791	0.760 .748-.771	0.708 .655-.762	0.689 .676-.701	0.731 .701-.762
4,096 context size	0.753 .727-.778	0.778 .768-.789	0.728 .682-.774	0.678 .665-.692	0.734 .707-.762
2,048 context size	0.729 .703-.755	0.880 .874-.886	0.722 .690-.754	0.654 .639-.669	0.746 .724-.769
1,024 context size	0.691 .666-.716	0.889 .883-.895	0.662 .626-.698	0.635 .620-.650	0.719 .696-.743
512 context size	0.658 .630-.686	0.820 .810-.829	0.631 .589-.674	0.609 .593-.625	0.679 .652-.707

Table 14 Performance for All Examples on EHRSHOT Across Time Windows. Area under the receiver operating characteristic curve (AUROC) performance and bootstrapped 95% confidence intervals for different time windows of the LLM embedding models and the count-based baseline.

Model	Operational Outcomes	Anticipating Lab Test Results	Assignment of New Diagnosis	Anticipating Chest X-ray Findings	Macro Avg. Across Task Groups
Qwen3-Emb-8B (4,096 tokens)					
Full patient history	0.772 .749-.795	0.866 .859-.873	0.705 .667-.743	0.674 .661-.688	0.754 .731-.778
3 years (1,095 days)	0.776 .753-.798	0.865 .858-.872	0.716 .671-.762	0.685 .673-.698	0.761 .734-.787
1 year (365 days)	0.788 .767-.810	0.865 .858-.872	0.720 .671-.769	0.702 .690-.714	0.769 .741-.796
1 month (30 days)	0.809 .790-.828	0.859 .852-.865	0.715 .666-.764	0.709 .698-.720	0.773 .746-.800
1 week (7 days)	0.818 .800-.837	0.851 .845-.858	0.687 .645-.729	0.690 .678-.701	0.762 .738-.785
1 day	0.809 .789-.830	0.823 .815-.830	0.736 .691-.781	0.657 .645-.670	0.756 .731-.782
1 hour	0.761 .737-.785	0.673 .663-.683	0.652 .610-.693	0.588 .573-.603	0.668 .643-.694
Qwen2-Emb-7B (4,096 tokens)					
Full patient history	0.771 .747-.795	0.865 .858-.873	0.716 .675-.757	0.666 .653-.680	0.755 .730-.780
3 years (1,095 days)	0.774 .749-.798	0.867 .859-.874	0.724 .685-.763	0.684 .672-.697	0.762 .738-.787
1 year (365 days)	0.792 .769-.814	0.867 .860-.874	0.702 .668-.737	0.699 .686-.711	0.765 .743-.787
1 month (30 days)	0.805 .784-.826	0.862 .855-.869	0.722 .673-.770	0.704 .693-.715	0.773 .746-.801
1 week (7 days)	0.809 .787-.830	0.856 .849-.863	0.719 .676-.762	0.687 .675-.698	0.768 .743-.792
1 day	0.813 .793-.833	0.826 .819-.833	0.743 .693-.793	0.657 .646-.669	0.760 .732-.788
1 hour	0.763 .737-.788	0.675 .666-.685	0.679 .641-.718	0.596 .581-.611	0.678 .654-.703
Llama3.1-LLM2Vec-8B (4,096 tokens)					
Full patient history	0.753 .727-.778	0.778 .768-.789	0.728 .682-.774	0.678 .665-.692	0.734 .707-.762
3 years (1,095 days)	0.767 .742-.792	0.780 .769-.790	0.708 .655-.761	0.690 .678-.703	0.736 .706-.767
1 year (365 days)	0.780 .757-.803	0.791 .781-.801	0.711 .660-.762	0.708 .696-.720	0.748 .719-.776
1 month (30 days)	0.798 .776-.820	0.821 .812-.829	0.733 .685-.781	0.715 .704-.725	0.767 .739-.794
1 week (7 days)	0.805 .783-.827	0.839 .832-.847	0.712 .664-.760	0.692 .681-.703	0.762 .735-.789
1 day	0.799 .776-.821	0.825 .818-.832	0.760 .717-.803	0.658 .646-.670	0.761 .735-.786
1 hour	0.758 .735-.780	0.668 .658-.678	0.658 .612-.705	0.592 .576-.607	0.669 .642-.697
Count-based + GBM					
Full patient history	0.774 .752-.797	0.728 .716-.741	0.719 .669-.768	0.656 .641-.671	0.719 .691-.748
3 years (1,095 days)	0.779 .757-.800	0.733 .720-.745	0.733 .692-.774	0.658 .645-.672	0.726 .701-.751
1 year (365 days)	0.788 .767-.809	0.738 .726-.750	0.729 .685-.773	0.677 .664-.689	0.733 .707-.759
1 month (30 days)	0.812 .792-.832	0.745 .733-.756	0.704 .666-.742	0.695 .684-.706	0.739 .716-.762
1 week (7 days)	0.821 .801-.840	0.749 .738-.759	0.695 .658-.732	0.691 .680-.702	0.739 .716-.761
1 day	0.824 .804-.843	0.729 .718-.740	0.711 .676-.746	0.657 .645-.668	0.730 .709-.752
1 hour	0.736 .711-.761	0.624 .614-.634	0.599 .552-.647	0.553 .538-.567	0.628 .600-.656

A.3 Additional Performance Results on EHRSHOT

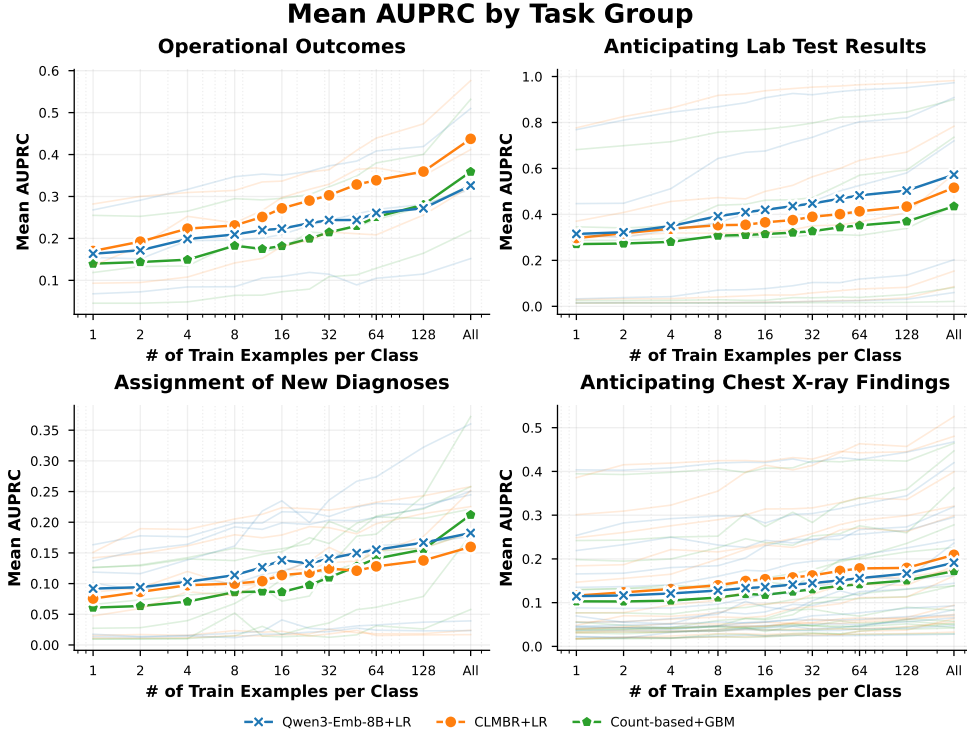


Fig. 9 Few-Shot AUPRC Performance on EHRSHOT. Mean area under the precision-recall curve (AUPRC) performance across subtasks for four task groups (bold). Blurred lines show averages across five bootstrapped runs using different seeds [44].

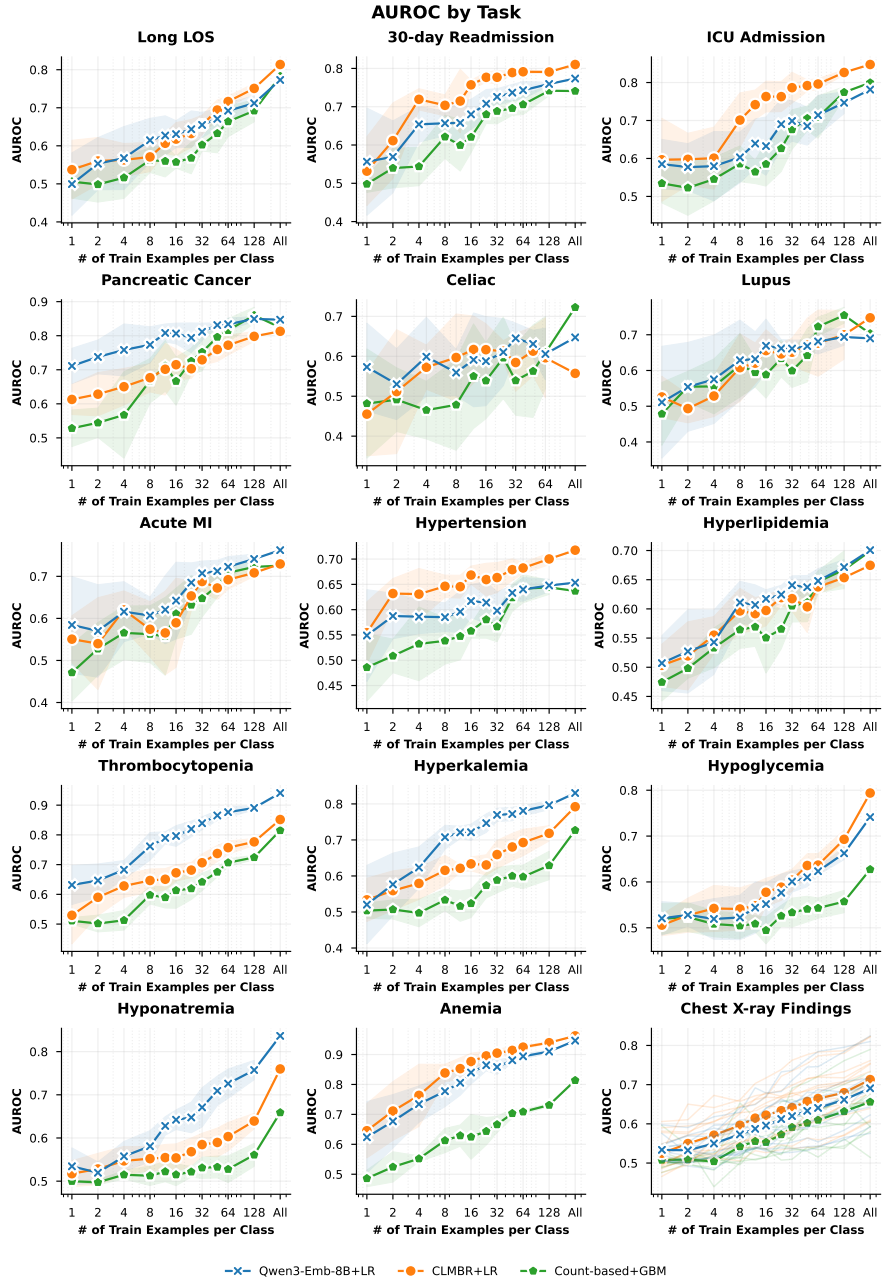


Fig. 10 Task-specific AUROC Performance on EHRSHOT. Area under the receiver operating characteristic curve (AUROC) performance with bootstrapped 95% confidence intervals across all 15 prediction tasks [44].

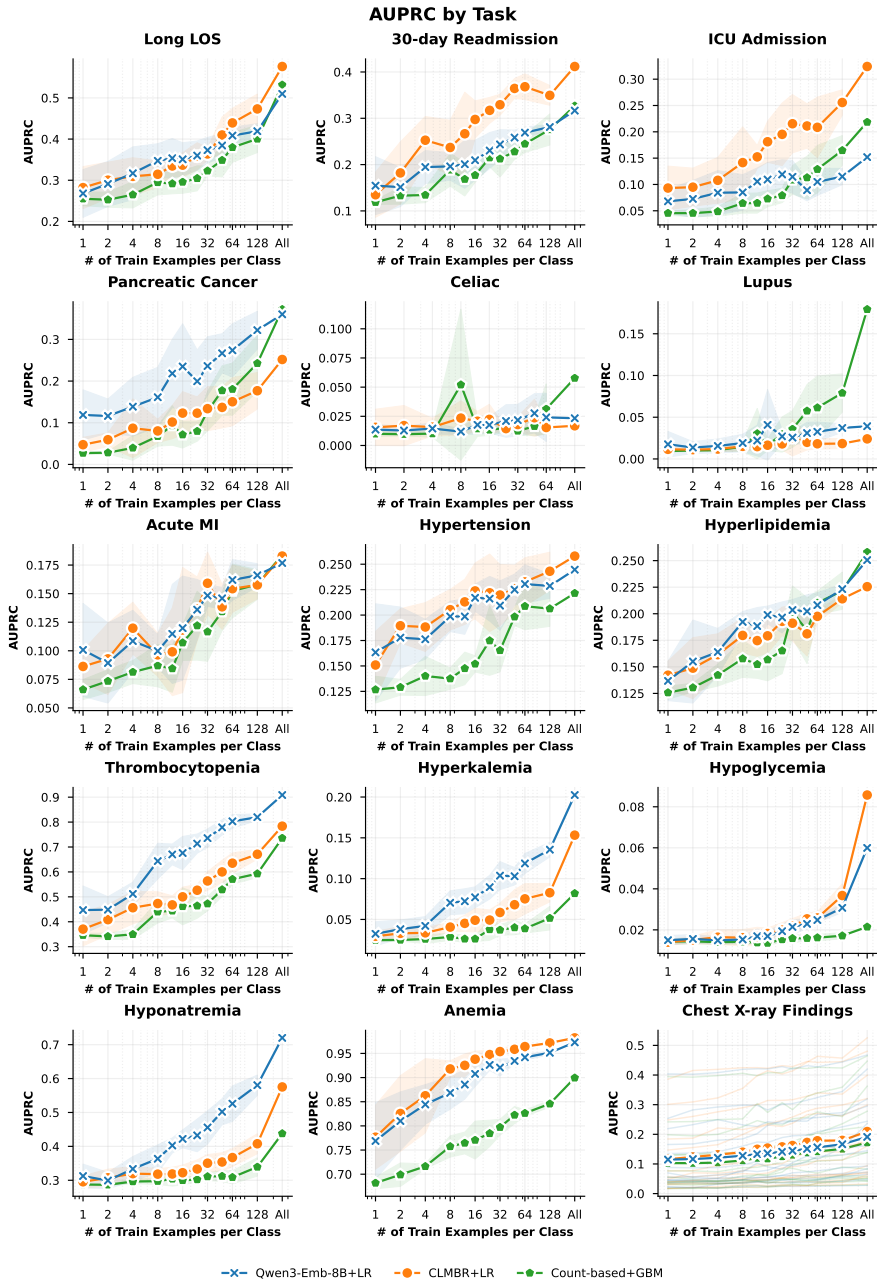


Fig. 11 Task-specific AUPRC Performance on EHRSHOT. Area under the precision-recall curve (AUPRC) performance with bootstrapped 95% confidence intervals across all 15 prediction tasks [44].

A.4 Additional Performance Results on UK Biobank

Table 15 Performance for All Examples on UKB. Mean area under the receiver operating characteristic curve (AUROC) performance and bootstrapped 95% confidence intervals for three task groups. The assignment of new diagnoses prediction is based on the mean of all 23 provided diseases. The macro-averaged performance across all task groups is given in the right-most column. All LLM embedding models use a context size of 8,192 tokens.

Model	Mortality prediction	Operational Outcomes (Hospitalization)	Assignment of New Diagnoses	Macro Avg. Across Task Groups
Baselines [44]				
CLMBR-T-Base	0.797 .779-.814	0.640 .628-.653	0.702 .687-.717	0.713 .698-.728
Count-based + GBM	0.738 .716-.760	0.627 .620-.635	0.699 .677-.721	0.688 .671-.705
LLM Embedding Models				
Qwen3-Emb-8B	0.840 .822-.858	0.673 .671-.675	0.732 .716-.748	0.748 .736-.760
Qwen2-Emb-7B	0.819 .804-.835	0.663 .660-.666	0.727 .712-.742	0.736 .725-.748
Llama3.1-LLM2Vec-8B	0.778 .765-.790	0.646 .638-.654	0.711 .696-.726	0.712 .700-.723

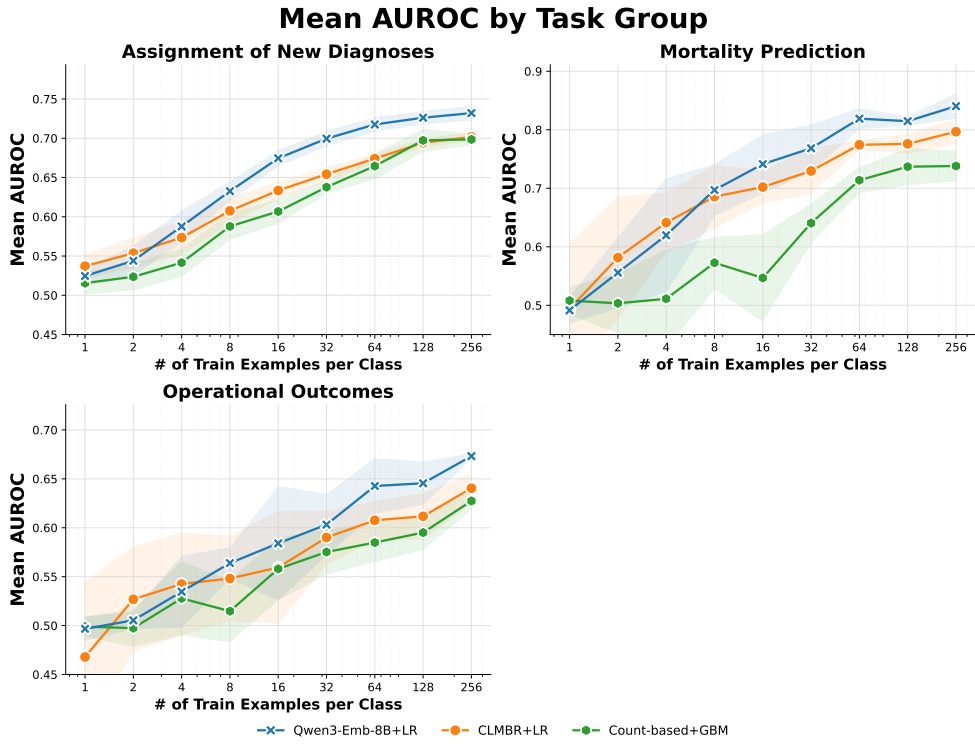


Fig. 12 Few-Shot AUROC Performance on UKB. Mean area under the receiver operating characteristic curve (AUROC) performance across subtasks for three task groups (bold). Blurred lines show averages across five bootstrapped runs using different seeds.

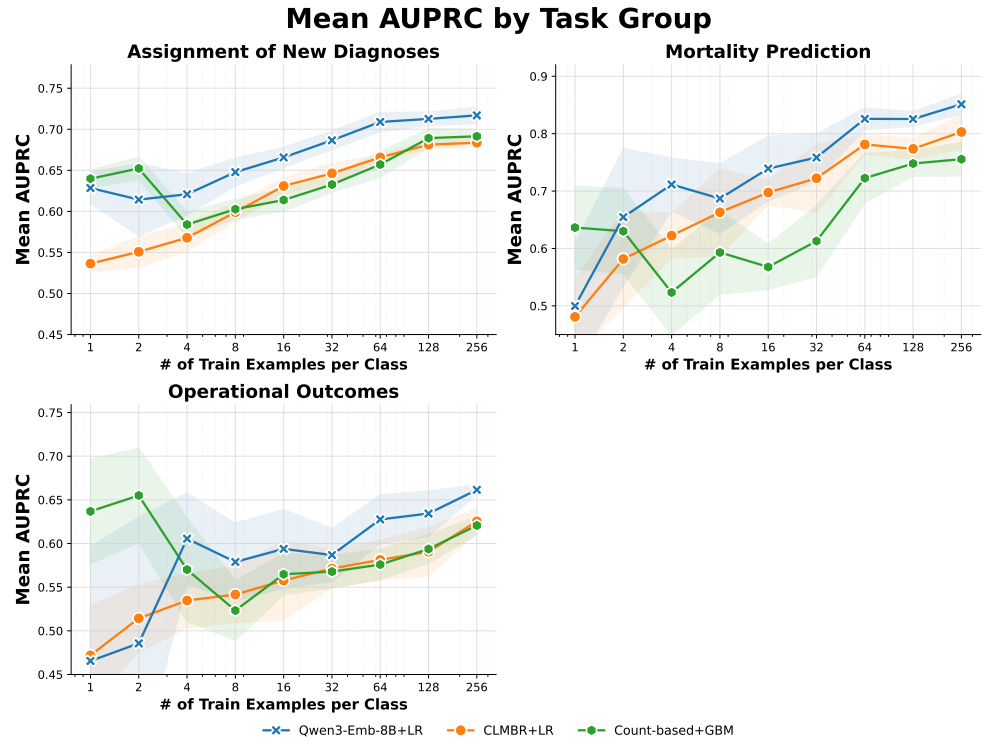


Fig. 13 Few-Shot AUPRC Performance on UKB. Mean area under the precision-recall curve (AUPRC) performance across subtasks for three task groups (bold). Blurred lines show averages across five bootstrapped runs using different seeds.

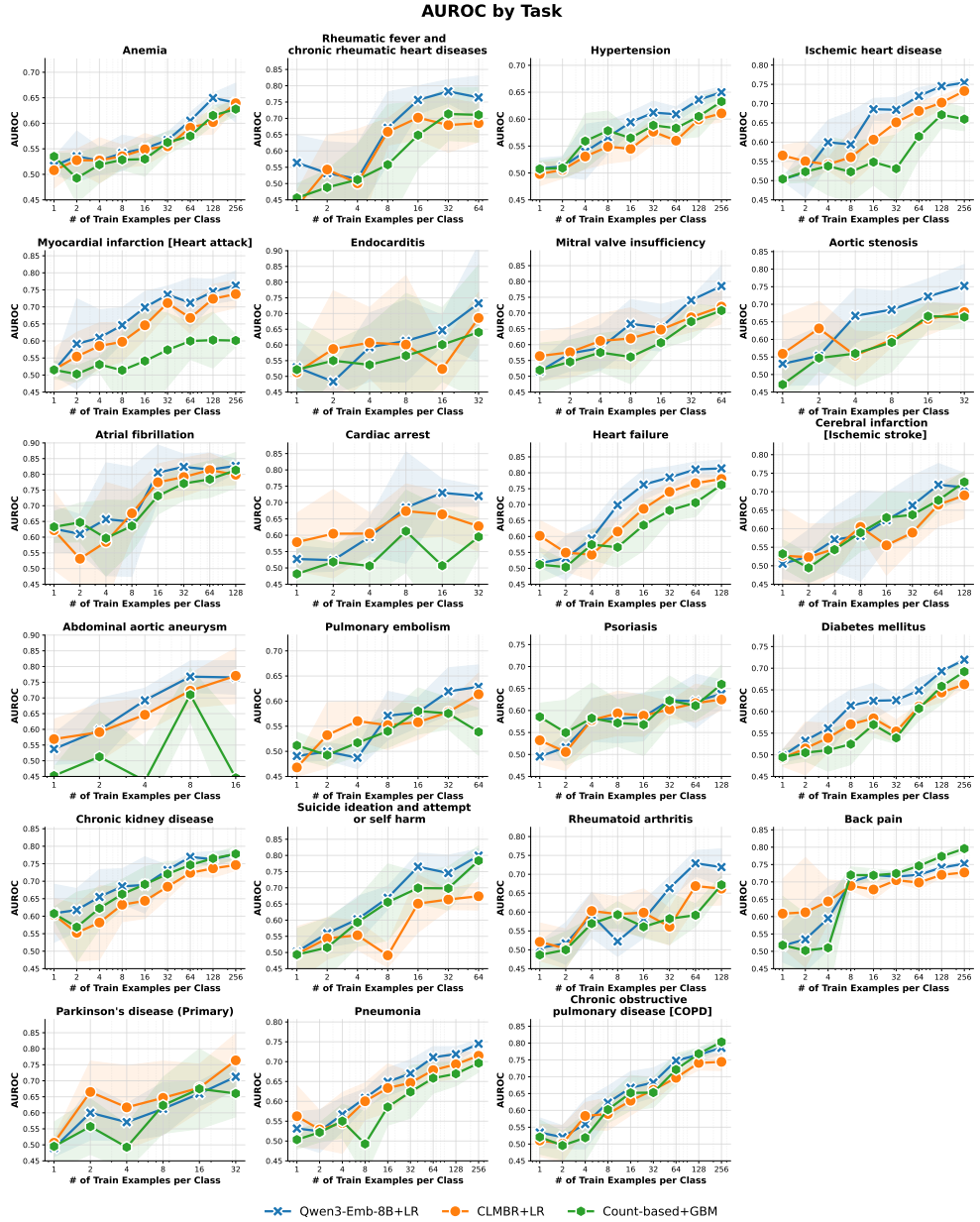


Fig. 14 Disease Onset AUROC Performance on UKB. Area under the receiver operating characteristic curve (AUROC) performance with bootstrapped 95% confidence intervals across the assignment of new diagnoses tasks.

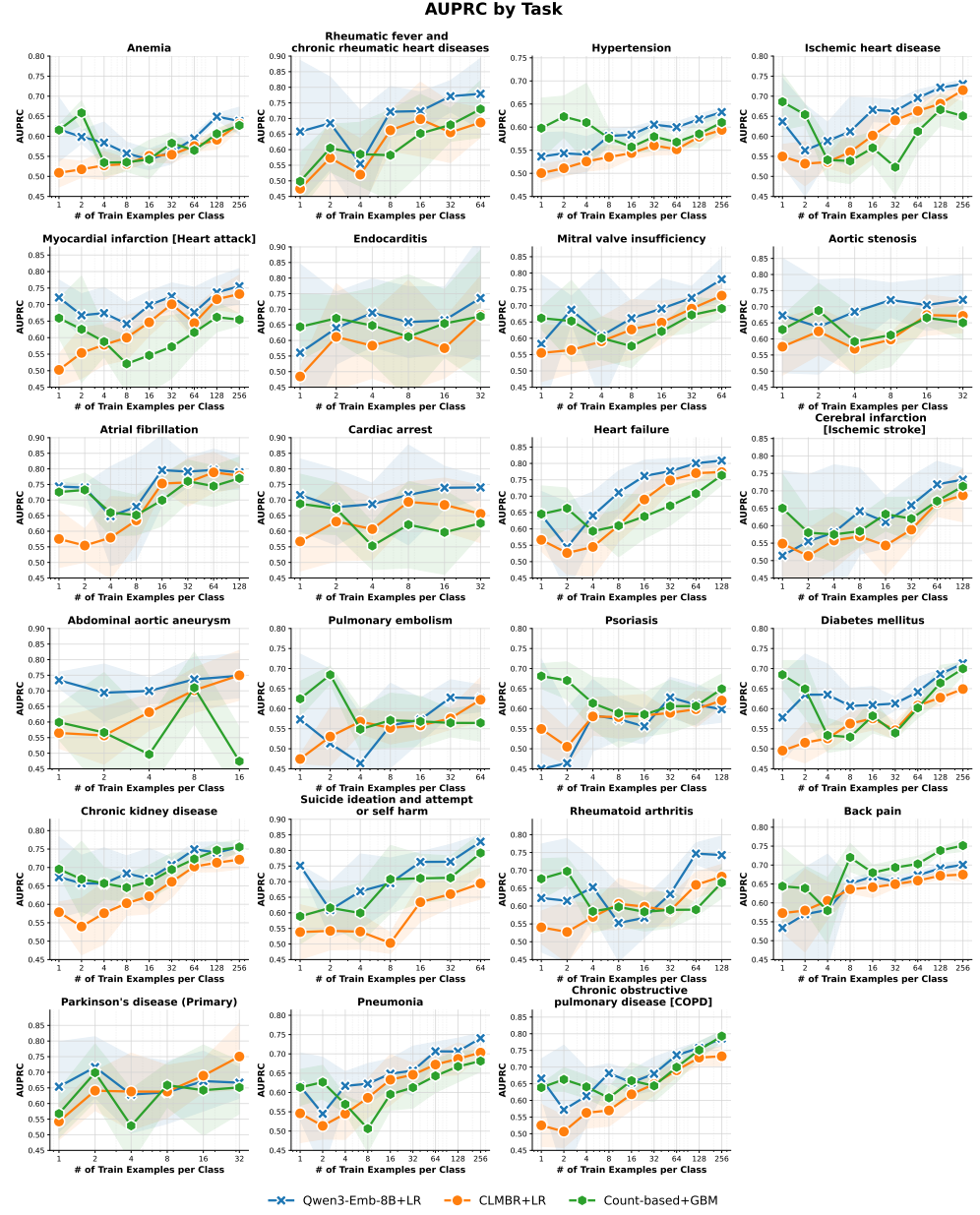


Fig. 15 Disease Onset AUPRC Performance on UKB. Area under the precision-recall curve (AUPRC) performance with bootstrapped 95% confidence intervals across the assignment of new diagnoses tasks.

A.5 Additional Performance For Encoder and Decoder Models

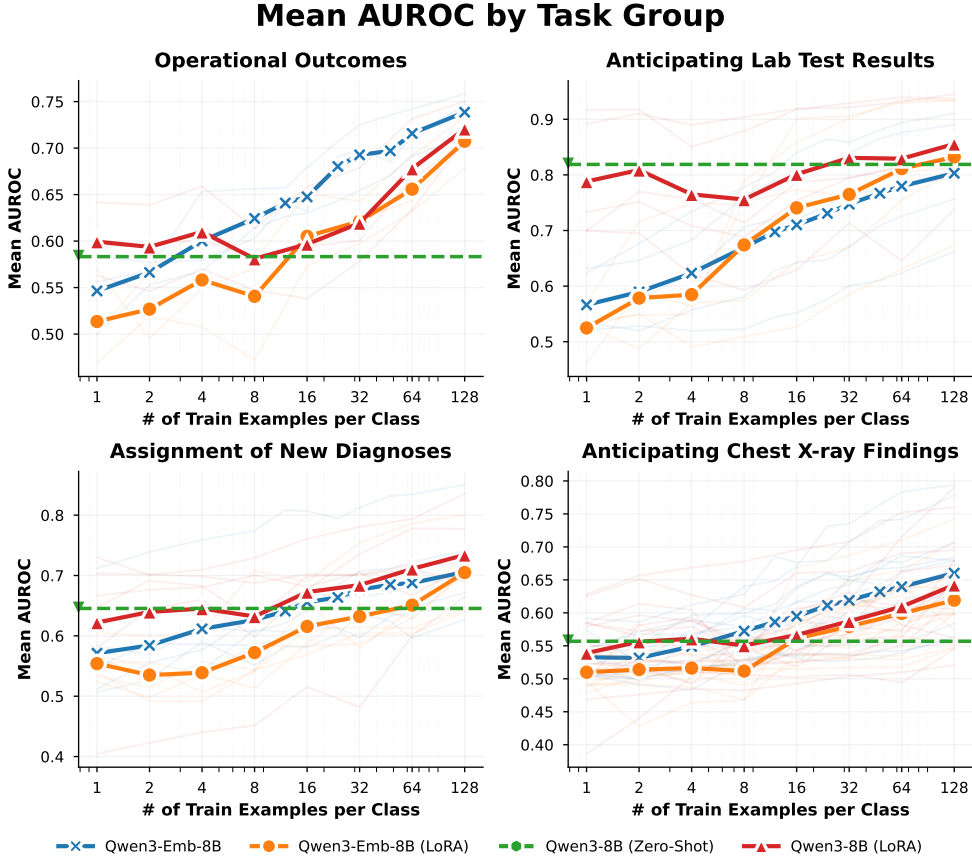


Fig. 16 Few-Shot AUROC Performance of Encoder and Decoder Models on EHRSHOT.
 Mean area under the receiver operating characteristic curve (AUROC) performance across subtasks for four task groups (bold). Blurred lines show averages across five bootstrapped runs using different seeds.

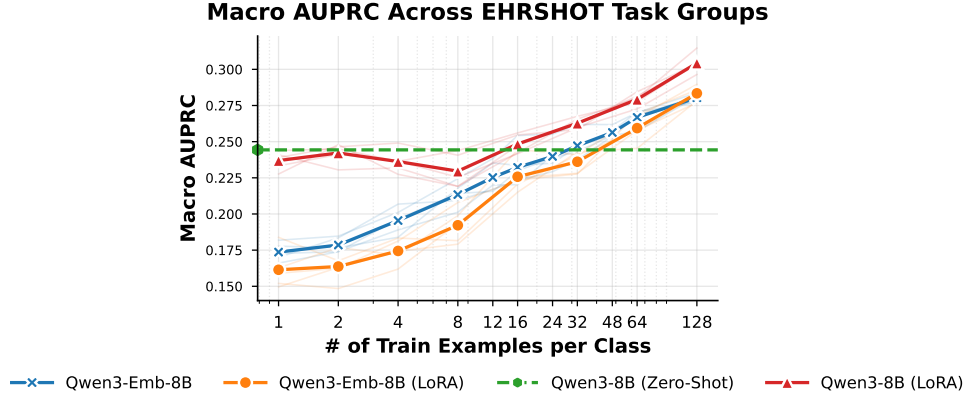


Fig. 17 Few-Shot AUPRC Performance of Encoder and Decoder Models on EHRSHOT. Macro-averaged area under the precision-recall curve (AUPRC) performance across all subtasks of EHRSHOT for zero to 128 training examples per class. Qwen3-Emb-8B is the encoder model used in this work (blue). We also tested a version fine-tuned end-to-end with LoRA (orange). Qwen3-8B is the decoder model with `Yes` and `No` tokens used for prediction. The decoder model is evaluated zero-shot (green) and after LoRA fine-tuning (red).

Mean AUPRC by Task Group

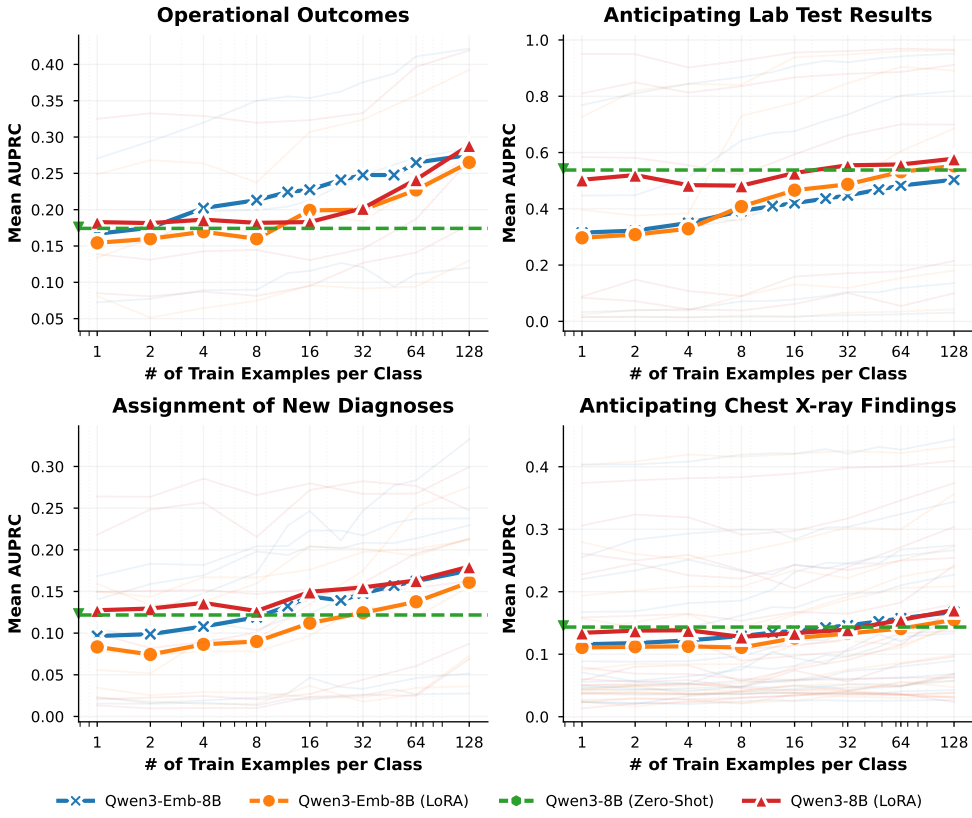


Fig. 18 Few-Shot AUPRC Performance of Encoder and Decoder Models on EHRSHOT.
 Mean area under the precision-recall curve (AUPRC) performance across subtasks for four task groups (bold). Blurred lines show averages across five bootstrapped runs using different seeds.